UC San Diego
UC San Diego Electronic Theses and Dissertations

Title

Structural_Health_Monitoring_of_Fatigue_Damage_to_Composite_Panels_Using_the_FailureForecast_Method_with_Positive_Feedback_Functions

Permalink

https://escholarship.org/uc/item/0528r8hb

Author

Ye, Jordan

Publication Date

2019

Peer reviewed|Thesis/dissertation

UNIVERSITY OF CALIFORNIA SAN DIEGO

Damage Prognosis with Embedded Fiber Bragg Gratings

A thesis submitted in partial satisfaction of the
requirements for the degree of Master of Science

in

Structural Engineering

by

Jordan J. Ye

Committee in charge:

      Professor Michael D. Todd, Chair
      Professor Charles R. Farrar
      Professor Kenneth J. Loh

2019

The Thesis of Jordan J. Ye is approved and is acceptable in quality and form for publication on microfilm and electronically:

_____

_____

_____

<div align="right">Chair</div>

University of California San Diego

2019

DEDICATION

In dedication to "The Gentle Art". Without jiu jitsu, I would not have the mental fortitude that helped me through my graduate studies at the University of California, San Diego.

EPIGRAPH

No man can reveal to you aught but that
which already lies half asleep in the dawning
of your knowledge.
If he (the teacher) is wise he does not bid
you to enter the house of his wisdom, but
leads you to the threshold of your own mind.
The astronomer may speak to you of his
understanding of space, but he cannot give
you his understanding.
And he who is versed in the science of
numbers can tell of the regions of weight and
measures, but he cannot conduct you hither.
For the vision of one man lends not its
wings to another man .

Kahlil Gibran, The Prophet

Compare yourself to who you were yesterday,
not to who someone else is today.

Jordan Peterson, 12 Rules For Life: An Antidote to Chaos

For it all depends on how we look at things, and not on how they are in themselves. The least of things with a meaning is worth more in life than the greatest of things without it.

Carl Jung, Modern Man in Search of a Soul

TABLE OF CONTENTS

LIST OF FIGURES

LIST OF TABLES

PREFACE

My journey through the graduate program has primarily been a way for me to test my limits. Upon partially finishing my studies at UCSD, I have proven to myself that I am capable of much more than what I had previously thought.

ACKNOWLEDGEMENTS

I would like to acknowledge Professor Michael D. Todd for his support as the chair of my committee. His leadership has always guided me in the right direction.

I would also like to acknowledge my previous boss Andrew Walker, for allowing me to work irregular hours so that I could attend lectures mid-day. Without his flexibility, I could not have had a smooth transition into the graduate program.

Finally, I would like to acknowledge Professor Jason Schweinsberg and Bruce Driver in the Mathematics Department at the University of California, San Diego who met with me to help me improve the technology administered in this paper.

VITA

2015	Bachelor of Science, University of California, San Diego
2015–2017	Project Engineer, QuEST Global Engineering
2017-2019	Grader, Department of Structural Engineering University of California, San Diego
2018–2019	Research Assistant, Department of Structural Engineering University of California, San Diego
2019	Master of Science, University of California, San Diego

PUBLICATIONS

"Composite Laminate Fatigue Damage Detection and Prognosis Using Embedded Fiber Bragg Gratings" Todd M, Gregory W, Key C, Yeager M, Ye J. ASME. Smart Materials, Adaptive Structures and Intelligent Systems, Volume 2: Mechanics and Behavior of Active Materials; Structural Health Monitoring; Bioinspired Smart Materials and Systems; Energy Harvesting; Emerging Technologies

FIELDS OF STUDY

Major Field: Engineering (Advanced Structural Analysis, Aerospace Engineering, and Structural Health Monitoring)

Studies in Mechanical Engineering
Professor Michael D. Todd

Studies in Civil Engineering
Professors Charles R. Farrar and Kenneth J. Loh

Studies in Materials Science and Engineering
Professor Kenneth J. Loh

Studies in Structural Health Monitoring
Professors Michael D. Todd, Charles R. Farrar, and Kenneth J. Loh

ABSTRACT OF THE THESIS

Damage Prognosis with Embedded Fiber Bragg Gratings

by

Jordan J. Ye

Master of Science in Structural Engineering

University of California San Diego, 2019

Professor Michael D. Todd, Chair

Structural health monitoring (SHM) has underwent great strides in system-level damage assessment. Now armed with advanced SHM strategies, engineers are attempting to forecast the remaining useful life within these same systems. SHM procedures that strive to predict failure is called damage prognosis. Damage prognosis predicts system-level performance by characterizing the structure's health, anticipating the future loads imposed onto the system, and finally forecasting the system's time of failure through repeated prognosis tests.

The SHM community has formulated a wide variety of well accepted prognosis designs and models. Although applicable across many systems, the investigation proposed here focuses on damage prognosis for submersible naval composite laminate material systems subjected

to dynamic loading. To validate the prognosis model, a series of mid-scale fatigue tests are performed on fiberglass reinforced plastic (FRP) panels. Embedded fiber Bragg gratings (FBG) periodically sample damage sensitive data from each panel. From the recordings, vibration based damage sensitive features are extracted and placed into a rate based time of failure assessment framework. Together, a positive feedback relationship and a failure forecasting method estimates the panel's remaining serviceability. Finally, a data driven statistical model produces probabilistic time of failure predictions.

One key objective is to prove the viability of using FBG sensors in a fatigue loading environment. Embedded FBGs have become more and more accepted as an embedded sensor concept for composites, but there are still research challenges surrounding their use. This work supports the motivation to integrate composite materials and embedded FBGs together for SHM of composites.

The other aim is to test a rate based SHM damage prognosis model. The underlying assumption to a rate based prognosis approach is that the evolution of a damage sensitive feature increases to infinity as failure is approached. The asymptotic behavior is called a positive feedback relationship. This work proves that fatigue growth obeys the positive feedback law and increasing feature rates can estimate failure.

In short, the results in this thesis showed that fiber optic sensors can be used in a fatigue loading environment and the positive feedback failure forecast method has potential to accurately predict time of failure.

Chapter 1

Introduction to Structural Health Monitoring and Rate Based Monitoring

1.1   Introduction

Ever since structures have been built, man has tirelessly asked, "Is my structure damaged?" To answer this question, our predecessors would then come up with means to test the integrity of their structures. One such test is called a tap test. Our predecessors would routinely tap their structures and compare the new observed sound with the original baseline tone. The tap would be the input signal, the sound would be the output signal, the tone would posses a damage sensitive quality, the ear would be the sensor, and the human nervous system would act as data acquisition (DAQ) system. Humankind has come along way since the creation of the tap test health monitoring. Though this technique is still used today, man has conceptualized creative solutions to the original question. These assessment strategies are called structural health monitoring (SHM). SHM is the study of designing specific strategies to detect damage as early as possible for aerospace, civil, and mechanical structures.[5]

Tones from tap tests do not provide a thorough structural health evaluation for every structural application. To that end, humankind has developed other non-invasive inspection techniques, which led to the Nondestructive evaluation field. Though, NDE has advanced damage detection remarkably in past decades, there still exists limits on NDE's capabilities for health monitoring; one being NDE techniques require the system to be taken offline. The need for an

implementable in-situ damage detection method has led to the formulation of SHM.

Today, engineers no longer need to rely on the five human senses to collect, interpret, and classify data. Advancements in electrical engineering and computer science has paved the way for state of the art sensing technology, computing hardware, and software algorithms. For example, an data interrogators can sample measurements of a structure's response more frequently and in greater detail than our five basic human senses ever could. Sensors are now even being fully embedded and instrumented into structures for a more homogeneous system. Cutting edge analyzers can transform recorded data in unique ways to reveal hidden damage related behaviors. Machine learning techniques can learn from data, identify patterns and make decisions with minimal human intervention.

The tremendous power in using SHM has been made possible because of the described technological advancements mentioned previously. An entire SHM damage detection system implements hi-tech components throughout its four-step process. Each step is necessary for monitoring to exist. Below is a itemized list of each step: [3] [4]

1. Operational Evaluation - Defines the damage to be detected and begins to answer questions regarding implementation issues for a SHM system.

2. Data Acquisition (DAQ) - Defines the sensing hardware and the data to be used in the feature extraction process.

3. Feature Selection - Identifies damage-related information from measured data.

4. Statistical Model Development - Classifies feature distributions into damaged or undamaged categories.

Once a structure's health has been determined, another follow up question is likely to be asked if one is particularly concerned about the structure's future performance. It is not uncommon to wonder, "What is the remaining life capability of my structure?" An approach to predict the remaining serviceability of a system is called damage prognosis.

This chapter will go over each of the four steps in greater detail and explain how they are applied to this research. Each step will be broken down into smaller specific components so the monitoring procedure can be thoroughly understood. First, the operational evaluation will be provided. Motivation for a damage prognosis system will be given, damage will be described, operational and environmental conditions are defined, and limitations on the DAQ are noted. Next, the DAQ system will be illustrated and the damage sensitive features will be characterized. Finally, the damage prognosis numerical methods and statistical framework will be depicted.

1.2 Structural Health Monitoring Overview

Figure 1.1. Virginia class submarine

In recent years, composite structures have been the driving force for better performing marine, aerospace, and civil structures. Composites have particularly been gaining popularity amongst US naval structural systems as composite material science and engineering capabilities continue to advance. For that reason, it has become important to also engineer real-time SHM assessment strategies to allow the designer to gain insight into these particular material systems. Advanced SHM systems help expand structural performance, organize operations, optimize maintenance planning, and reduce overall life cycle costs.[3]

This thesis was worked under Small Business Innovation Research (SBIR) N111-053. The SBIRs overall goal is to invent a SHM protocol capable of detecting, characterizing, and

assessing the damage in submersible composite components. Phase I introduced the damage detection scheme and sensing setup. In Phase I of SBIR N111-053, Michael Yeager created a binary hypothesis-based impact damage detection scheme for composite material systems.[42] He combined a passive fiber optic sensing system with a vibration based damage detection approach. After mid-scale impact tests, the Phase I SHM system was shown to be a success. This thesis extends Yeager's work with developments made by Barry Voight and Joseph Corcoran. With Michael Yeagers work serving as a stepping stone, Phase II explores different approaches in using rate-based failure forecasting methods. [12] [17] Yeager's SHM approach is assimilated into Voight's positive feedback failure forecasting method by using a rate-based integrated SHM system. Together, a detection, assessment, and prognosis SHM system will be created and verified on mid-scale vibration tests. A distinction must be made at this point in the thesis. The onboard SHM system proposed for naval submersible vessels is not the same as the test SHM system that will be used during the experiments. These distinctions will be made clear throughout the rest of the thesis where applicable.

1.2.1   Operational Evaluation

The operational evaluation defines the damage to be detected and begins to answer questions regarding implementation issues for a SHM system. A well planned operational evaluation will: [3] [4]

1. Provide economic and/or life-safety justification for performing the monitoring.

2. Define system-specific damage including types of damage and expected locations.

3. Define the operational and environmental conditions under which the system functions.

4. Define the limitations on DAQ in the operational environment.

Aside from research purposes, funds will not be allocated towards advancing a SHM scheme if there is not a present need for one. Providing an economic and/or life-safety justifica-

tion gives motivation to having a SHM system. Once a program necessitates monitoring, other aspects of the operational evaluation can be called for. A properly tailored SHM arrangement can be created granted that probable damage modes, probable damage locations, critical damage levels, damage evolution time scales, operational condition, environmental conditions, and DAQ limitations are well understood. An even better fitting SHM protocol can be developed if these same observations are quantifiable. Defining the problem at hand as much as possible will help guide the remaining steps of the four step SHM procedure. It may not be obvious how the operational evaluation sets up the monitoring scheme for success right now, but it will be obvious later on how decisions made in later steps comeback to defined parameters in the operational evaluation.

Motivation

Advancements in design and analysis techniques have proven that multi-constituent systems are advantageous if applied appropriately. One example of such systems are composite structures. Composites have high strength and stiffness material properties. They can also be tailored to a desired configuration to efficiently reduce weight. When compared to their metallic counterparts, FRPs are also corrosion resistant.

Unfortunately, composite material science cannot guarantee safety. Complex failure modes that are not fully understood accompany all the added benefits of using composites. Manufacturing such structures is also labor intensive and their manufacturing defects are equally troublesome. Likewise, finding these failure initiation sites is difficult, costly, and time consuming. Even with strong finite element models paired with advanced testing schemes, there is little that engineers can do to fully understand a composite structure's behavior subjected to the aforementioned complexities.

Embedded SHM systems allows engineers to uniquely understand the complex mechanics of such structures. Changes within the structures can be detected and predicted if SHM systems are used correctly. Observed behavioral tendencies can later be used to improve designs and

lower the risk involved with using composites. In performance sensitive vehicles like naval structures, significant weight can be spared and the cost associated with that weight can be reduced as well. Maintenance and overall component life cycle cost can also be lowered if engineers know when parts need to be repaired or replaced.

Though the cost saving operations related to the SHM systems are valued, they are not the primary reason for a detection and assessment plan of submersible naval composite components. The main objective of an on-board SHM system is to help ensure homeland security. Naval vehicles help guard our nation through surveillance and defense operations. Taking a naval structure offline for a routine inspection puts national security at risk. By incorporating an active SHM system to constantly diagnose a structures condition, improved serviceability of naval vehicles can effectively transpire. Critical decisions made by the Department of Defense (DoD) and the Department of Homeland Security (DHS) to safeguard the nation will have the strong backing of the SHM assessment protocol.

Damage

Possible fatigue damage modes include, matrix cracking, delamination, bolt bearing damage, crack formation, crack propagation, and boundary condition weakening, all of which can adversely affect the system's performance. In terms of the damage sensitive feature, these forms of damage are interrelated with a system's physical properties. The mass, damping, and stiffness properties will change when damage is present and change the structure's dynamic response

Operational and Environmental Conditions

The operational and environmental conditions on the fatigue tests are different from the actual operational and environmental functioning conditions. When in fleet service, the composites will face hydrodynamic loads, varying sea-states, environmental dynamics,and engine vibrations. The composite may also face loads from impacts, but this severe condition is

not being modeled in this thesis. Only the natural loads are being considered. During testing, the test specimens will face, ambient air environmental dynamics and a sinusoidal dynamic load applied by a shake table. The ambient air environmental dynamics are assumed to be negligible.

Limitations on DAQ

The limitations on the DAQ during the fatigue tests are different from the limitations on the DAQ during the functioning conditions. The strains realized during fatigue testing phases were too large for the DAQ system to record, and therefore the sensors could not monitor each test specimen during damage propagation. Because the testing procedure hasn't been addressed, it may not be clear how this affects the SHM protocol. More will be reported on this operational constraint later. The limitation does not affect the functioning SHM system. The environmental and operational ambient loads on the composite during naval operations are far below the applied loads during testing, and therefore the sensors could be used to monitor the submersible composite component at all times during naval operations.

1.2.2 Data Acquisition

Data acquisition (DAQ) defines the sensing hardware that records system observations. Careful planning goes into the DAQ system due to its multifaceted problem and multistage procedure. To simplify the entire measurement process, a DAQ system can be divided into six different parts: 1.) Excitation; 2.) Sensing; 3.) Data Transmission; 4.) Analog to Digital Conversion; 5.) Data Storage; 6.) Data Cleansing, Normalization, Compression, and Fusion.
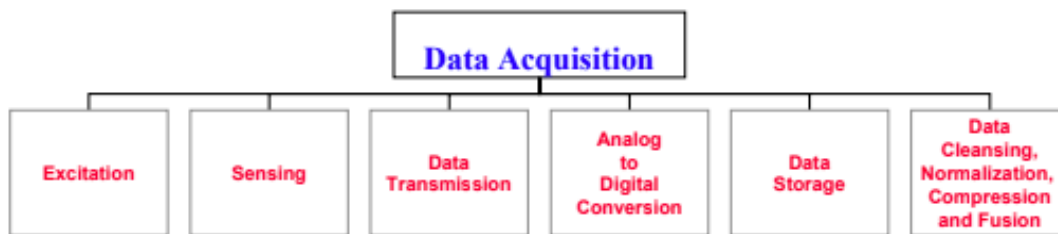
Figure 1.2. The six separate parts of data acquisition.

To begin defining the DAQ system, several system-level constraining questions must be asked: [3] [4]

1. What features will be extracted from data for SHM assessment?

2. What factors may need to be considered for accurate assessment?

3. What will be used: active or passive sensing?

4. Are there any overall imposed limitations or constraints on what systems can be used?

First, imposed economical, political, and environmental constraints are considered. They will put restrictions on the DAQ system and eliminate other recipes altogether. The DAQ system is then shaped by the strongest options out of the remaining possibilities because having a powerful and finely-tuned DAQ system is crucial for a strong SHM protocol. Theoretically if all other steps in the SHM process are well thought out, the SHM results will be heavily dependent on the gathered data; therefore it is pertinent that the recording system makes accurate and precise measurements. Other data management procedures are often added into the DAQ system to uncover the damage sensitive response from extraneous noise or bias. Some steps include data cleansing, normalization, compression and fusion, just to name a few.[5]

Engineers also turn to the operational evaluation to answer the system level constraining questions. The operational evaluation can rule out certain methods and favor other. For example, certain damage specifications might support some sensing technologies over others. Each sensing scheme may then require its own special power, networking, and bandwidth demands. Additionally, particular active sensing excitation signals may have the backing from the environmental conditions. Operational conditions could determine when data collection occurs or whether a passive sensing approach would be a better option than an active approach.

After answering all the system-level constraining questions and defining the DAQ components, a comprehensive DAQ system will be formed. A well planned DAQ system will:

1. Define the type of data to be acquired.

2. Define the sensor type, number, locations, bandwidth, and sensitivity.

3. Define the DAQ, transmittal, and storage system.

4. Define the power source for the system.

5. Define when data collection will occur.

6. Define the excitation signal and source.

7. Establish a data normalization procedure.

8. Define a data cleansing regimen.

9. Define a data compression procedure.

The data acquisition setup for the mid-scale vibration tests is as follows. First, a band-limited white noise excitation signal is created by a function generator in MATLAB. This excitation simulates a pseudorandom operational loading that is representative of what would be experienced by a component in service at sea. The signal is sent to a National Instruments cDAQ-9178 data acquisition system that sends the output voltage to a MB Dynamics SL500VCF power amplifier. The power amplifier controls a leveled 25 lb. MB Dynamics shaker that is connected to the test specimens by a plastic rod. While the panel is being excited by the shaker, a Micro Optics Hyperion Platform si155 optical interrogator powers the fiber optic sensing system and records the output wavelength response readings from the FBGs. Out of the eight test specimens, two had embedded fiber optics that were underneath one ply of fiberglass. The other sensors were attached to the exterior surface with epoxy resin. The data is finally stored on a laptop.

A similar DAQ arrangement could be used for the functioning SHM protocol. Because the ambient loads on the composite are assumed to be BLWN, the ambient loads could act as the

excitation signal. This convenience means that a passive sensing approach could be used and the entire excitation process could be eliminated. Only the interrogation and data storage system would be required. Furthermore, sensors could be embedded farther beneath the surface of the composite structures during the manufacturing process.

Embedded Fiber Optic Sensors

Many have emphasized the added benefits of embedded sensing systems. Nondestructive evaluation (NDE) researchers encourage integrated sensor due to their convenience. Although NDE techniques such as, e.g. ultrasonic scan, X radiography, acoustic emission method, and passive thermography are effective in damage detection, they are inconvenient due to their tendency to mandate that the system be taken offline to utilize such NDE techniques.

Permanently installed sensors allow engineers to orchestrate SHM without taking the system offline. Ideally, permanently installed sensors will be used for real-time monitoring procedures to provide the best time domain resolution of the DAQ system. For this thesis in particular, they will help to track behavioral trends used in prognosis by taking frequent measurements. The specific embedded sensors in this thesis also facilitate a non-intrusive, robust, and efficient sensing system. [19] [20]

Structures with integrated sensors have been called "smart structures" and the demand for smart structures has paved the way for fiber optic strain gauges. Fiber optic sensors are small, lightweight, immune to electromagnetic fields, and resistant to corrosion. [19] Initially, many were skeptical about the feasibility of embedded fiber optics, especially their integration into composite structures. By far, one of the most important concerns while integrating fiber optics within composite structures is their influence over the structural integrity of the composite part. [26] [27] [28] [29] [30] [31] [32] Composites already have sophisticated behaviors, complex failure modes, troublesome manufacturing defects, and difficult repair practices. Adding internal interactions with a sensor may aggravate these complexities causing the mechanical properties to become diluted with the presence of stress concentrations and material inhomogeneity. New

failure modes may also emerge which further increases the probability for premature failure.

It had been hypothesized that reduction in performance will be a function of the optical fibers orientation, the thickness of the structure running along the fiber, and the fiber optic diameter. Experiments from Siavouche Nemat-Nasser showed that the sensors did in fact affect the initiation of failure and the development of damage, but the material properties and tensile strength of the composite structure remained unaffected by sensor inclusions.[21] Kunigal Shivakumar, and Legunchim Emmanwori showed that structural tensile strength degradation becomes increasingly detrimental as the angle between the optical fiber and ply directions becomes more severe. They witnessed that the tension failure initiation mode presented itself as a fibermatrix separation at the ends of the resin pockets around the fiber optic sensor. In compression, the final failure ended with fiber microbuckling and kinking. The fiber optic increased composite fiber misalignment and therefore decreased the compression strength by as large as 40%. [22] [23]

Though all of the above composite microstructural changes and variables are relevant, recent research has shown that some embedded fiber optics will not compromise composite structures. The sensors tested in the previous studies by Nasser, Shivakumar, and Emmanwori had diameters that were significantly larger than the average composite ply thickness. Now, fiber optics can be manufactured with diameters on the scaled of micrometers. Small diameter optical fibers, i.e. 125 μm or less, have been shown to not affect composite strength or damage actualization what so ever. [24] [25]

The sensors used in this thesis were custom made to have a diameter close to 125μm. Though sensor structural/interaction would not be a concern, part of the work in this thesis is to confirm that fiber optic strain gauges could be used as a fundamental sensing component for the SHM solution.

Fiber Bragg Gratings

Though fiber optics sensors come in a range of sizes, there is one commonality among all sensing systems of this type: fiber optics exploit the use of waveguided light to interact with the environment in a way to produce a measurement of an intended physical measurand, e.g., strain, temperature, etc. Lights reflective and refractive properties are applied to detect strain values. The most basic optical fiber strain gauge consists of two distinct regions: the core and the cladding. The core is usually made out of glass or silica and is the region in which light is contained. Surrounding the core is the protective cladding. The cladding is often times made of a plastic material that has a lower density than the core. The interface where the two different materials meet serves to minimize transmission of light, achieve total internal reflection, and channel the light inside the fiber when light is passed through the fiber core.

Schematic diagram of a fiber Bragg grating.
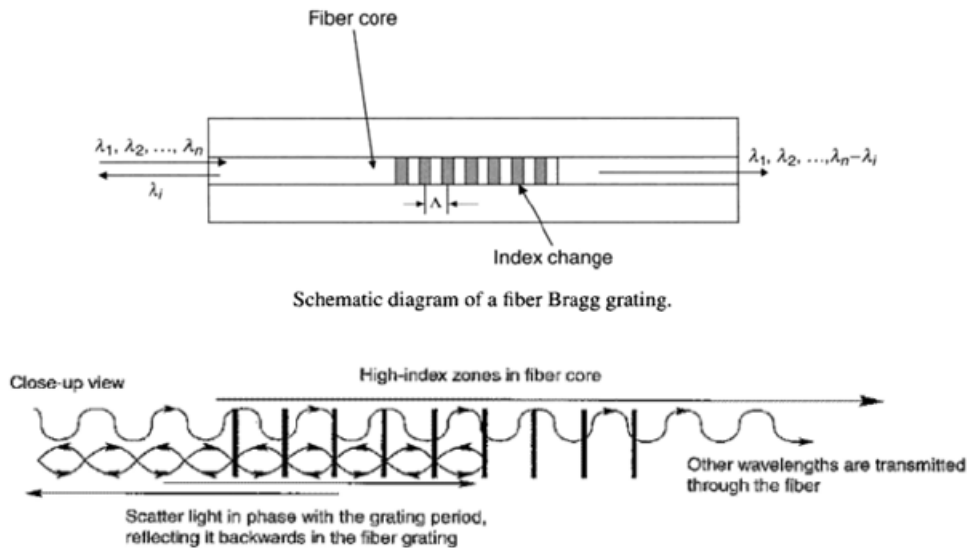
Figure 1.3. Fiber Bragg grating

The fiber core and the cladding themselves cannot produce the strain reading. They only serve the purpose to transmit the light to and from the sensor and the interrogator. Fiber Bragg gratings (FBGs) are the sensing mechanism. FBGs are discontinuities that are inscribed into the fiber during the fibers production. They are a periodic modulation of the index of refraction of

12

the core. Index of refraction is defined below:

$$n = \frac{V_{vacuum}}{V_{medium}} \tag{1.1}$$

where:

$n > 1$

V_{vacuum} = The speed of light in a vacuum

V_{medium} = The speed of light in a medium

Without the FBGs, a broadband light signal will transmit through undisturbed. The FBGs act as disturbances in the light's path that filters the passing broadband light input at distinct points along the fiber optic. The different FBG material interfaces will block a narrow band reflection at distinct wavelengths of light and pass other wavelengths of light through. As the light continues to pass through successive FBGs, different reflections will materialize at gratings down the fiber optic. In simpler terms, different material interface discontinuity spacings will reflect a different wavelength of light.
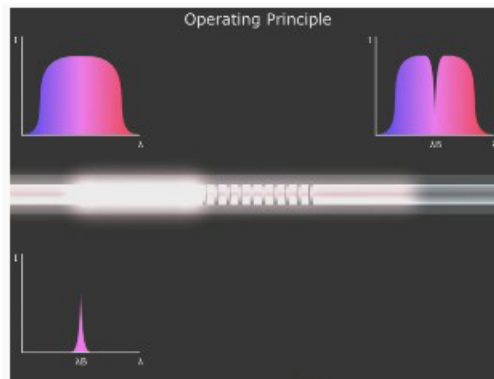
Figure 1.4. Single FBG reflection

The flexibility in FBG spacings brings into light another benefit to using optical strain gauges. Many different sized gratings can be installed inside one optical fiber. This concept is called frequency division multiplexing and is the most common approach used today. Each
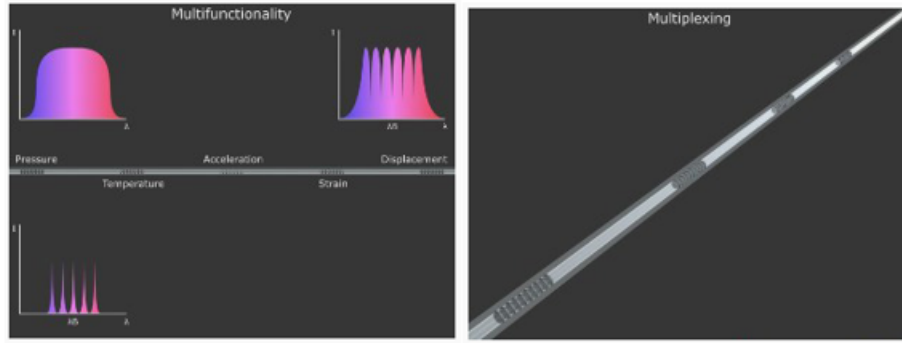
Figure 1.5. Frequency division multiplexing

grating will have a different Bragg grating pitch, and a different wavelength of light will be reflected when a continuous laser light source is emitted into the fiber optic. When the fiber is deformed, the gratings will change orientation due to the strains developed and a perturbed wavelength of light will be reflected back to interrogator. Recordings of reflected wavelengths of light are indicative of local strains at FBG locations. The equation for the wavelength to strain conversion is as follows:

$$\frac{\Delta\lambda}{\lambda_0} = (1 - P_e) * \varepsilon + (P_e * (\alpha_s - \alpha_f) + \zeta) * \Delta T \tag{1.2}$$

where:

$\Delta\lambda$ = Wavelength shift

λ_0 = Nominal (Initial) wavelength

P_e = Strain-optic coefficient (Sensitivity)

Sensitivity = Ratio of the fractional change in electrical resistance to the strain

ε = Strain

α_s = Thermal expansion coefficient for bonding material

α_f = Thermal expansion coefficient for optical fiber

ζ = Thermo-optic coefficient (describes the change in refractive index due to ΔT)

ΔT = Change in temperature
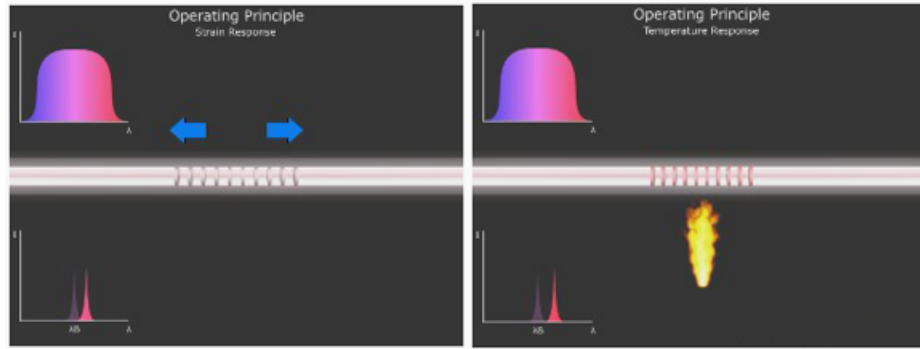
Figure 1.6. Strain and temperature effects

There are a few key takeaways to be noted here before proceeding any further. First of all, it is important that an FBG's reflected wavelength range does not overlap with another FBG's spectral range. If this is the case, the interrogator will have a difficult time discerning what nominal wavelength the shift belongs to. Effects of this problem will coalesce into erroneous strain value readings associated with large deviations from the true strain. This complication ties back to the limitations on the DAQ system. The strains realized during fatigue testing phases created overlaps in the FBGs' spectral ranges, and therefore the fiber optics sensors could not monitor each test panel during damage propagation.

It is equally important that the light is contained within the fiber optic. If refraction leakage occurs between the core and cladding, the broadband input may lose frequency content which is within the narrow band reflection of an FBG. When leakage occurs, the FBG, and more over the strain value, will be passed over.

1.2.3   Feature Selection

So long as the fiber optic sensors and DAQ arrangement function as intended, the third step in the SHM process can begin: feature selection. Interestingly enough, one must have a general idea of what the damage sensitive feature will be prior to planning the DAQ system. Having a general idea of what the feature will be can help determine what response will be collected and how measurements will be taken. The damage sensitive feature will be extracted

from the DAQ recordings so it is important that the DAQ system is somewhat tailored to the feature. Damage is defined as changes to the material and/or geometric properties of a structural system, including changes to the boundary conditions and system connectivity, all of which can adversely affect the system's performance. The process of deciding what measured response characteristic is used to indicate damage is called feature selection. Feature selection is a crucial step in SHM for a number of reasons. Feature selection can influence the DAQ arrangement. A unique feature may determine what types of data will be collected and how measurements will be taken. Another reason why feature selection is an important process is that some features will be more fitting than others. A well selected feature will: [3] [4]

1. Transform data into useful information.

2. Be very sensitive to damage and insensitive to extraneous factors other than damage.

3. Have well defined sources of variability.

4. Have the lowest dimensionality as possible.

There are multiple approaches in finding a damage sensitive feature. If someone has had experience with similar monitoring problems, past experiences could help in deciding what would be an appropriate feature option for the problem at hand. Another way to select a feature is to first conduct multiple numerical simulations of a damaged system's response and then validate the simulations through system level testing. Once a firm understanding of a system's response due to varying damage levels is established, a damage sensitive feature can be picked. System level testing alone could also construct the same damage level/response relationship.

Assuming that the DAQ system is well structured, varying damage levels will be monotonically followed by correlated responses. The feature values should also have values parallel to the damage levels. Ideally features should increase or decrease with increasing damage levels. Unfortunately, this is not always the case. Often times the selected feature is sensitive to damage but also moderately sensitive to extraneous values. Though the overall feature behavior follows

16

the structure's health, incidental influences can have an effect over the feature value that makes feature interpretation more opaque.

The best corrective action for extraneous factor sensitivity is to understand their influence on the feature. If the impact of extraneous factors can be quantified, uncertainty bounds can be established on the feature values and feature values can be interpreted more descriptively.

When a strong feature has been chosen from feature selection, feature extraction can begin. Feature extraction is the process of drawing the damage related information out from the measured data. Signal and data processing techniques may be needed to excavate the damage sensitive information. Some techniques include Fourier transforms, data compression, and data fusion. These processes can alter the dimensionality of the feature. Dimensionality determines how much data is required for a desired level of statistical confidence. Low dimensional features are desirable because accurate confidence levels in feature distributions can be obtained from less data. Furthermore, low dimensional features require less computing power to work with. Unfortunately, in attempts to decrease feature dimensionality, substantial system health level information may be lost in the reduction process. High dimensional features require considerably large amounts of data to establish adequate confidence levels in feature distributions. SHM systems that gather large amounts of data, like continuous monitoring programs or complex SHM arrangements, may be able to work with higher dimensional features.

Two different damage prognosis methods are being tested in this thesis:

- Direct Method - Uses feature values for damage prognosis

- Indirect Method - Uses feature rate values for damage prognosis

The most obvious choice for a feature would be to examine the surveyed strain distribution. If the applied load is constant and increasing strains are recorded, the panels stiffness could be degrading or the panel itself could be increasing in length. Unfortunately, this feature choice has high dimensionality and is sensitive to extraneous factors. Thermal strains may contribute to

17

the overall recording, and in this thesis, changes in temperature are not categorized as damage. Noise in the recording may also bias the strain values.

Vibration Based Damaged Identification

A unique set of damage sensitive features have emerged with the rising interest of integrated sensors. Vibration based features, like modal parameters, are now being explored in the SHM damage detection field. The use of advanced vibration based damage identification has been made possible because of advancements in sensing technology, fast Fourier transform analyzers, and computing hardware. Vibration based features help to provide a global structural health assessment that NDE cannot provide. NDE requires prior knowledge of damage locations. Evaluation could take a long time if the area is large. Additionally, NDE requires access to the vicinity of damage. If access is not possible, the structure must be taken offline to disassemble the system in order to gain access.

Embedded fiber optics paired with vibration based features provide a holistic damage detection strategy that doesn't require disassembly, system shut down, or a priori damage location knowledge. The fundamental motivation behind vibration based features is that system-level modal parameters are interconnected to a system's global physical properties like mass, damping, and stiffness. Damage can be detected through changes in the modal properties when damage degrades these physical characteristics and changes the dynamic response the feature is derived from. The works of Doebling, Sohn, and Farrar set the stage for vibration based damage detection. [33] [34] [35] [36] Montalvao and Kessler went on to apply their works to composite structures. [37] [38]

Two common modal analysis classes appeared from extensive research in vibration based damage detection. One category is called experimental modal analysis (EMA). The other is known as Operational Modal Analysis (OMA). [39] In EMA the excitation input and output response is known. Both are used in vibration based damage detection. This arrangement would require an active sensing system that sends out an active excitation signal and records the output

response signal. In OMA only the output response is known. OMA can still solve for the modal properties given that the excitation is stochastic and broadband (e.g. white noise). This thesis uses an active sensing system to model a passive sensing system. For the submersible naval vessel this SHM protocol is being customized for, it is assumes that the environmental and operational loading together can be modeled as white noise. For this reason, the excitation signal is white noise to match the assumption, and EMA and OMA are one in the same. Furthermore, traditional frequency response function methods (FRF) can still be used. The tests performed use an active approach but the actual application of this SHM will be passive.

Cross Power Spectral Density Prominent Peak Shifts

The feature chosen follows that which was proposed by Yeager in Phase I of SBIR N111-053.[42] Like many others, Yeager chose a vibration based damage sensitive feature. Damage is assumed to manifest itself in the system's mass, stiffness, and damping. Changes in these physical properties also alter the structure's dynamic response and FRF. As more damage is introduced, resonant frequency peaks will situate at lower frequencies than their baseline values. Shifts in the structural FRFs are used as the damage sensitive feature.

Identifying the resonant frequency shifts takes place through finding spectral densities. There exists a special case of the FRF when the input is known to be white noise. White noise is a special type of signal. For any point in a white noise signal, the present value is completely correlated to itself and completely uncorrelated to any past or future values of the white noise signal. For this reason, the autocorrelation function for a white noise signal is then represented as a dirac delta function. There is complete correlation when the time delay between two points is zero and there is no correlations when the time delay between two points is any finite value.

First, the auto-correlation and cross-correlation function must be defined. Below is the definition of the autocorrelation function.

$$\phi_{xx}(t_1, t_2) = E[x(t_1)x(t_2)] = \int_{-\infty}^{+\infty} \int_{-\infty}^{+\infty} x_1 x_2 f_{x_1 x_2}(x_1, t_1, x_2, t_2) \, dx_1 \, dx_2 \qquad (1.3)$$

where:

$\phi_{xx}(t_1, t_2)$ = The autocorrelation function

$E[]$ = The expectation of a function

$x(t_1) = x_1$ = A random variable or signal realization at time t_1 belonging to random process or signal $x(t)$

$x(t_2) = x_2$ = A random variable or signal realization at time t_2 belonging to random process or signal $x(t)$

$f_{x_1 x_2}(x_1, t_1, x_2, t_2)$ = Joint probability density function of x_1 and x_2

The autocorrelation function is the similarity of a signal with a delayed copy of itself. If one time is represented as time shift away from the other time, the autocorrelation function could better be represented as a function of a time delay. To solve for the autocorrelation between t_1 and t_2, the expected value of the product of $x(t_1) = x_1$ and $x(t_2) = x_2$ must be found. The complete autocorrelation function is then an entire description of the autocorrelation between any two times or any time delay. The function indicates how much the present value of the process depends on the past values of the process and also indicates how much the future values of the process depends on the present value of the process. The auto correlation function is a function of two different times of a time delay.

Equally, the cross-correlation function is the similarity of a signal with a delayed copy of another signal. If one time is represented as a time shift away from the other time, the cross-correlation function could better be represented as a function of a time delay. To solve for the cross-correlation between t_1 and t_2, the expected value of the product of $x(t_1) = x_1$ and $y(t_2)$ = y_2 must be found. The complete cross-correlation function is then an entire description of the cross-correlation between any two times or any time delay. The function indicates how much the present value of the process depends on past values of another process and also indicates how much the future values of the process depends on the present values of the another process. Below is the definition of the cross-correlation function:

$$\phi_{xy}(t_1,t_2) = E[x(t_1)y(t_2)] = \int_{-\infty}^{+\infty} \int_{-\infty}^{+\infty} x_1 y_2 f_{x_1 y_2}(x_1,t_1,y_2,t_2)\,dx_1\,dy_2 \qquad (1.4)$$

where:

$\phi_{xy}(t_1,t_2)$ = The cross-correlation function

$E[]$ = The expectation of a function

$x(t_1) = x_1$ = A random variable or signal realization at time t_1 belonging to random process or signal $x(t)$

$y(t_2) = y_2$ = A random variable or signal realization at time t_2 belonging to random process or signal $y(t)$

$f_{x_1 y_2}(x_1,t_1,y_2,t_2)$ = Joint probability density function of x_1 and y_2

The power spectral density (PSD) and cross power spectral density (CPSD) are the Fourier transform of the autocorrelation function and cross-correlation function. For a continuous time series, signal, or random process, $x(t)$, the Fourier spectrum, also known as the Fourier transform $X(f)$), is defined as:

$$X(\omega) = \frac{1}{2\pi} \int_{-\infty}^{+\infty} x(t)e^{-i\omega t}\,dt \qquad (1.5)$$

where the signal is defined from $-\infty$ to ∞ and

$i = \sqrt{-1}$

ω = Angular frequency (rad)

t = Time (s)

The Fourier transform of a signal describes the signal in terms of its amplitude, phase shift, and frequency. Generally, the Fourier transform of of a random process $x(t)$ is called the spectral decomposition of a random process. The inverse Fourier transform is as follows:

$$x(t) = \int_{-\infty}^{+\infty} X(\omega)e^{i\omega t}d\omega \qquad (1.6)$$

To reiterate, the PSD and CPSD are found by taking the Fourier transform of the autocorrelation and cross-correlation function respectively. The PSD is as follows:

$$\hat{\phi}_{xx}(\omega_1, \omega_2) = E[X(\omega_1)X(\omega_2)] = (\frac{1}{2\pi})^2 \int_{-\infty}^{+\infty} \int_{-\infty}^{+\infty} \phi_{xx}(t_1, t_2)e^{-i(\omega_1 t_1 - \omega_2 t_2)}dt_1\,dt_2 \qquad (1.7)$$

where:

$\hat{\phi}_{xx}(\omega_1, \omega_2)$ = The power spectral density

$E[]$ = The expectation of a function

$X(\omega_1)$ = The value (complex) of the spectral decomposition of $x(t)$ at ω_1

$X(\omega_2)$ = The value (complex) of the spectral decomposition of $x(t)$ at ω_2

$\phi_{xx}(t_1, t_2)$ = The autocorrelation function

The autocorrelation function and the PSD form a Fourier transform pair called the Wiener-Khintchine relation. The Wiener-Khintchine relation states that the fourier transform of the autocorrelation function is the PSD and the inverse Fourier transform of the autocorrelation function is the PSD. Similarly, the cross-correlation function and the CPSD also form a Fourier transform pair.

$$\hat{\phi}_{xy}(\omega_1, \omega_2) = E[X(\omega_1)Y(\omega_2)] = (\frac{1}{2\pi})^2 \int_{-\infty}^{+\infty} \int_{-\infty}^{+\infty} \phi_{xy}(t_1, t_2)e^{-i(\omega_1 t_1 - \omega_2 t_2)}dt_1\,dt_2 \qquad (1.8)$$

where:

$\hat{\phi}_{xy}(\omega_1, \omega_2)$ = The cross power spectral density

$E[]$ = The expectation of a function

$X(\omega_1)$ = The value (complex) of the spectral decomposition of $x(t)$ at ω_1

$Y(\omega_2)$ = The value (complex) of the spectral decomposition of $y(t)$ at ω_2

$\phi_{xy}(t_1, t_2)$ = The cross-correlation function

The PSD of the white noise autocorrelation function would be the Fourier transform of a dirac delta function. The Fourier transform of a dirac delta function is a constant function. It makes sense that white noise has a constant PSD function because white noise has equal intensity at all frequencies meaning that its Fourier transform is also constant valued.

The FRF is generally represented in two way: 1.) The ratio of the ouput response Fourier transform to the input excitation Fourier transform; and 2.) The ratio of the CPSD between the input and output to the PSD of the input.

$$H(\omega) = \frac{Y(\omega)}{X(\omega)} = \frac{\hat{\phi}_{xy}(\omega_1, \omega_2)}{\hat{\phi}_{xx}(\omega_1, \omega_2)} \tag{1.9}$$

where:

$H(\omega)$ = The frequency response function

$X(\omega)$ = The Fourier transform of a known input $x(t)$

$Y(\omega)$ = The Fourier transform of a known output $y(t)$

$\hat{\phi}_{xy}(\omega_1, \omega_2)$ = The cross power spectral density

$\hat{\phi}_{xx}(\omega_1, \omega_2)$ = The power spectral density

With the white noise assumption, the FRF can be simplified. White noise signal has a Fourier transform and a PSD that is constant valued, and the FRF can be directly characterized by the output response or the CPSD between the input excitation and output response.

Yeager chose to use the CPSD, but not between the input excitation and output response. Yeager chose a damage sensitive feature that used the CPSD between two output responses at two different FBG sensor locations.

The cross-correlation of two different output responses describes the similarity between one output response at one FBG location with another output response at a different FBG location. Taking the Fourier transform of this cross-correlation function would lead us to the CPSD between the two different output responses. But, if the Fourier transform of an FBG's output response due to white noise is the FRF at that particular sensor location, the CPSD between the two responses would effectively be a cross-correlation function between the FRFs at the two FBG locations. In other words, the CPSD between the two output responses would effectively compare how similar the FRFs at two different sensor locations are to each other.

As the structure incurs damage, the individual FRFs will all have resonant frequencies that shift to lower frequency values than their baseline positions. Likewise, the CPSD plots will also have prominent peaks that situate at lower frequency values. The amount of shift in the prominent peaks of the CPSD plots compared to the baseline CPSD plots will be indicative of damage.

Damage Sensitive Feature and Feature Rate

Because multiple peaks could exist, the feature at this point is multidimensional. Yeager reduced the multidimensional feature by reducing all the peak shifts to a working scalar metric called the Mahalanobis distance.

Each observed peak shift was assembled into a multivariate feature array.

$$x = [\Delta_1, \Delta_2, \Delta_3, ..., \Delta_k] = argmax[\hat{S}_{ij}^0[\omega_{0,k}]] - argmax[\hat{S}_{ij}^d[\omega_{d,k}]] \tag{1.10}$$

where there exists k number of peaks between the ith and j^{th} sensor pair.

$\hat{S}_{ij}^0$ = CPSD for the ith and j^{th} sensor pair for the baseline structural state

$\hat{S}_{ij}^d$ = CPSD for the ith and j^{th} sensor pair for the damaged structural state

$\omega_{0,k}$ = Frequency CPSD peak locations for the baseline structural state

$\omega_{d,k}$ = Frequency CPSD peak locations for the damaged structural state
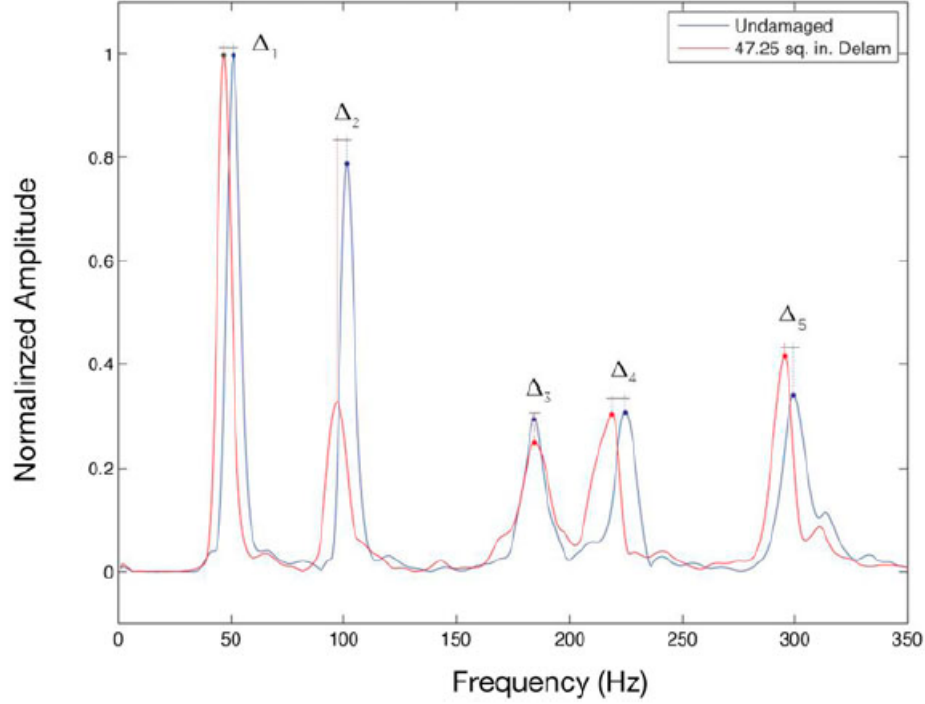
Figure 1.7. Example of resonant frequency peak shifts. [42]

The multidimensional feature set is then reduced to the working scalar feature metric called the Mahalanobis distance. In order to compress the feature, the covariance of the data from the baseline training set is required. The compression process will be described in greater detail in Chapter 3.

$$\Omega_i = (x_i - \bar{x})^T \Sigma^{-1} (x_i - \bar{x}) \tag{1.11}$$

where:

Ω_i = The Mahalanobis distance

x_i = Feature vector for a damaged structural state

$\bar{x}$ = Mean of feature vectors from the baseline training set

Σ = Covariance matrix of the baseline training set

The damage sensitive feature is the Mahalanobis distance of the prominent peak shifts between the damaged and baseline CPSD of the output strain responses from two different sensor pair locations. As the structure incurs more damage, the Mahalanobis distance will increase in value.

1.2.4 Statistical Model Development

The Mahalanobis distance damage sensitive feature can finally be placed into a statistical framework once the damage sensitive feature extraction has been properly orchestrated. System health evaluation will depend on advancements made in feature selection and extraction. A feature's value, uncertainty, variability, and dimensionality will make clear distinctions about the system's health, and is only made possible by statistical models. The statistical model development process classifies feature distributions into definitive categories. A well planned statistical model will: [3] [4]

1. Determine if the system is damaged. (Damage Detection)

2. Determine the location of present damage.(Damage Localization)

3. Characterize the type of damage present.(Damage Characterization)

4. Determine the extent of damage present.(Damage Quantification)

5. Determine the remaining useful life of the structure. (Damage Prognosis)

The feature's statistical properties are utilized in structural health decision making during the final step of the four step SHM procedure. In general, there are two types of machine learning approaches that help in making an informed decision: 1.) Unsupervised Learning and 2.) Supervised Learning. Both models attempt to answer the question, "Does this feature value come from its undamaged state or its damaged state?" [5]

Answering this question becomes a difficult process when there is no data from the undamaged state. In this case, an unsupervised machine learning algorithm must be used and a novelty detection statistical model is typically chosen. If the statistical model incorporates information from the undamaged and damaged cases, a supervised learning style is being used, and typically a group classification or regression analysis is chosen. Health assessments are made based on the feature deviating away from undamaged feature values in the feature space. Generally, supervised approaches are easier to work with than unsupervised approached. In supervised learning, more information about damage variability is established. If more damage classifications are known and the classifications are well separated in the feature space, a more detailed damage categorization system can exist. [6] [7]

It is important to mention here that having a well defined operational evaluation and feature will help to have a stronger statistical model. The primary role of the statistical model is to differentiate between damage related changes and non-damaging events. Some non-damaging events are:

- Test-to-test variability

- Unit-to-unit variability

- Environmental and operational variability

- Data transformation variability

If a damage sensitive feature is chosen strategically and its variability is well understood, not only can the feature space be interpreted, but decoding statistical changes in the feature space and making conclusion about the structure will also be easier. Some further conclusions could be damage location, extent, and type.

These consequences take shape in false-positive and false-negative results. False-positive results will indicate damage when none is present, where as false-negative results will not indicate damage when damage is present.

As mentioned previously, a well instituted hypothesis test can help to provide fitting statistical interpretations of results. Depending on the problems a statistical model faces, the hypothesis test can be personalized to do one of three things: 1.) Reach a correct SHM assessment with the least probability of false-positive and false-negative errors; 2.) Minimize the sample size required before a correct decision is made; 3.) To accept or reject inconclusive results as the sample size increases and any observed difference is because of the error produced by non-damage events. It is important to note that all three goals cannot be met. The first goal could be chosen if false-negative and false-positive results produce catastrophic results. The second goal could be chosen if acquiring data is difficult or time is of the essence. Finally, the third choice might be chosen if there is large observed variability in the data set.

Picking one of the three fashioned hypothesis test objectives ties back to having a strong operational evaluation, DAQ system and feature. If all are well planned and well understood, there will not need to be a compromise on the three conflicting goals because the hypothesis test will be clear and conclusive with a high probability of being correct. Only when there are gaps in the SHM procedures will a choice need to be made. Perfectly designing a SHM procedure is difficult. To that end, compromises will need to be made throughout the process and particular approaches will be favored over others. For the problem surrounding false results of naval submersible vessels, a statistical model that reaches a correct SHM assessment with the least probability of false-positive and false-negative errors is best.

Yeager developed a false-assessment binary hypothesis statistical model in his SBIR N111-053 Phase I SHM efforts.[42] He saw that the Mahalanobis distance-squared feature values follow a chi-square distribution, and therefore established a confidence level baseline threshold. If a Mahalanobis distance-squared feature value exceeded the threshold, the feature data point would be categorized as damaged. If the squared feature value was within the threshold, the feature data point would be categorized as undamaged. Each sensor pair would then randomly select a feature data point from the most recent impact damage level, assess the feature value, and categorize the health of the structure as healthy or unhealthy. In his test, a false-negative

28

result would be a point that comes from the damaged structure but is labeled as undamaged and a false-positive result would be a point that comes the undamaged structure but is given a damaged assignment. After choosing a 95% confidence threshold and cross checking the statistical model with the test data from all performed damage levels, sensor pairs never made false-negative assessments and made less false-positive assessments as impact damage increased.

This thesis takes parts of Yeager's existing SHM solution and tests a prognostics algorithm with his damage detection SHM plan. His statistical model was successful in assessing a structure's health due to impact damage, but its practicality in assessing a structure's health due to fatigue damage has not been investigated. Advanced statistical categorization of the feature space like Yeager's is not used in this thesis. Instead, a series of feature categories within the feature space were created out of necessity. Feature values and time of failure predictions that fit these categories were disregarded from prognosis. First, since time is a nonnegative number, any negative time of failure prediction was ignored. Equally, any rates that were calculated as negative were ignored. This choice is in line with the underlying assumption of the method of using a positive feedback feature that are positive and increase to infinity. A negative damage sensitive feature rate would imply a self-healing panel. Finally, data from sensor pairs that did not indicate significant damage were ignored and only data from the ten sensor pairs with the largest signs of damage were considered. Sensor pairs that did not strongly indicate damage also did not strongly indicate that the damage sensitive feature rate was increasing to infinity.

1.3 Damage Prognosis, Positive Feedback Functions, and The Failure Forecast Method

Once a statistical model evaluates the current damage state of the system, damage prognosis can begin. Damage prognosis is defined as an attempt to:[8] [9] [10] [11]

> "...forecast system performance by assessing the current damage state of the
> system (i.e. SHM), estimating the future loading environments for that system,
> and predicting through simulation and past experience the remaining useful life

of the system."

Damage prognosis is the pinnacle of SHM. Being able to predict failure has enormous potential, but is by no means an easy task. If done incorrectly or inaccurately, damage prognosis can have life-threatening and costly consequences. In the case of damage prognosis, conservative will forecast failure sooner than what will actually occur, where as non-conservative predictions will forecast failure later than what will actually occur. To conduct damage prognosis, we must reexamine the feature and feature rate.

The damage prognosis procedures used in this thesis were first discovered by Barry Voight.[12] [13] [14] [15] [16] Voight believed that a positive feedback function could model volcanic failure in which the entire system had an underlying unstable feature that evolved asymptotically to infinity. Where the asymptote is located in time would be the point of volcanic eruption. His objective was to:

> (1) introduce a fundamental relationship describing pre-eruption rate changes of various phenomena; (2) develop equations that couple rate changes of volcanic processes to the time of event occurrence; (3) emphasize the predictive utility of the inverse representation of rate; and (4) apply the predictive method to examples of several specific eruptions.

He then went on to verify and validate his model with geodetic observations, seismic quantities, and geochemical observations of different volcanoes. For five separate eruptions, the failure forecast methods predictions coincided with actual eruption dates. More importantly, predictions with high confidences levels could be made earlier than what was formerly possible. He coined the term "failure forecast method" for the predictive strategy he cultivated. Little did he know that his study in the failure forecast method would spur great strides in SHM damage prognosis.

Joseph Corcoran realized the power of Voight's work as a positive feedback mechanism and showed how rate-based monitoring can enable prognosis.[17] [18] Corcoran extended Voights work to rate based SHM of fatigue, creep crack growth, and volumetric creep damage mechanisms. He used other positive feedback mechanisms forms different than Voights original

postulate to accommodate a particular failure mode in question. Furthermore, Corcoran's work also strongly stresses the use of permanently installed sensing systems with rate based SHM. Permanently installed sensors allows for frequent measurements which lead to improved rate calculations. With accurate feature rate data and unique failure forecasting methods, his models predicted fatigue, creep crack, and volumetric creep failure more accurately than predictions made by forcing Voight's model upon a particular failure behavior.
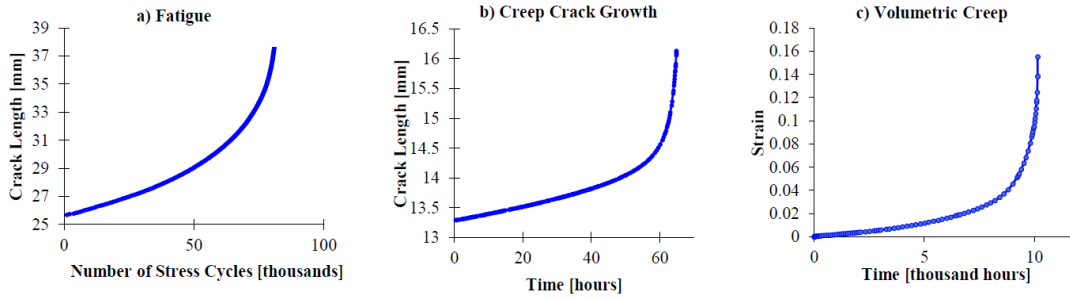
Figure 1.8. Examples of positive feedback mechanisms.[17]

This thesis is another attempt to verify and validate the work of Voight and Corcoran. [12] [17] Voights original model will be applied to predict panel failure due to fatigue loading. Two approaches are generated and tested. Voight started with and used the power law positive feedback function. This relationship is as follows:

$$\dot{R}(t) = \kappa * R(t)^{\alpha} \tag{1.12}$$

where:

κ = A scaling constant relevant to a specific physical process

$R(t)$ = The rate of change(R(t)) of an observed feature Ω

α = The Power Law's exponent relevant to a specific physical process.

The differential equation can be solved for Ω. First let us write the power law in terms of Ω:

31

$$\frac{d^2\Omega}{dt^2} = \kappa * \frac{d\Omega}{dt}^\alpha \tag{1.13}$$

Let $\frac{d\Omega}{dt} = v(t)$, $\frac{d^2\Omega}{dt^2} = \frac{dv(t)}{dt}$, and rearranging the equation to solve for κ:

$$\frac{dv(t)}{dt} * v(t)^{-\alpha} = \kappa \tag{1.14}$$

Integrating both side with respect to t:

$$\frac{v(t)^{-\alpha+1}}{-\alpha+1} = \kappa * t + c_1 \tag{1.15}$$

Solving for $v(t)$

$$v(t) = {}^{-\alpha+1}\sqrt{-(\alpha-1)*(\kappa*t+c_1)} \tag{1.16}$$

where c_1 is some scalar constant. At time of failure, the observed rate is infinite ($v(t_f) = \frac{d\Omega(t_f)}{dt} = R(t_f) = \infty$). Likewise, the inverse of the observed rate at failure would be zero. Constant c_1 can be solved by applying the asymptotic boundary condition.

$$\frac{1}{v(t_f)} = \frac{1}{{}^{-\alpha+1}\sqrt{-(\alpha-1)*(\kappa*t_f+c_1)}} \tag{1.17}$$

where:
$$c_1 = -\kappa * t_f - \frac{R_f^{1-\alpha}}{-1+\alpha}$$

Integrating both side of the equation with respect to t and applying the boundary condition that at time 0 the feature value is some scalar number $\Omega(0) = \Omega_0$ allows us to arrive at the general feature solution equation:

$$\Omega(t) = \Omega_0 + \frac{-(R_f^{1-\alpha} - \kappa*(t-t_f)*(-1+\alpha))^{\frac{2-\alpha}{1-\alpha}} + (R_f^{1-\alpha} + \kappa*t_f*(-1+\alpha))^{\frac{2-\alpha}{1-\alpha}}}{\kappa*(-2+\alpha)} \tag{1.18}$$

where:

Boundary Condition 1 : $\Omega(0) = \Omega_0$

Boundary Condition 2 : $\frac{1}{\dot{\Omega}_f} = \frac{1}{R_f} = 0$

$\dot{\Omega}_f = R_f = \infty$

R_f = Feature rate at failure time $t = t_f$

$\Omega(t)$ = Feature value

Ω_0 = Feature value at time $t = 0$

1.3.1   Rate Value Method-"Indirect"

The general rate solution can be derived by taking the derivative of the general feature solution equation:

$$R(t) = (R_f^{1-\alpha} - \kappa * (\alpha - 1) * (t - t_f))^{\frac{1}{1-\alpha}} \tag{1.19}$$

At the time of failure, the observed rate would be infinite or the inverse of the observed rate would be zero. We arrive at the following equation after applying the asymptotic boundary condition to the inverse problem and the following condition where:

$R(t_c) = R_c$

R_c = The rate of change of an observed feature at a given current time t_c

t_c = The current time of an observed feature rate

$$t_f = t_c + \frac{R_c^{1-\alpha}}{\kappa * (\alpha - 1)} \tag{1.20}$$

where:

t_f = Time of failure

After Voight's analysis to verify and validate his model, he saw that his data fit reasonably well with a simplified form in which α equals two. If α were assumed to be two, a linear relationship would exist.

$$-\kappa * t_c + \kappa * t_f = \frac{1}{R_c} \tag{1.21}$$

The previous resembles $m * x + b = y$, and therefore, time of failure could be found by fitting a line between points of known times(t_c) and feature rates(R_c). After the slope(κ) and the intercept($\kappa * t_f$) is solved for, time of failure can be found by dividing the intercept by the slope. The indirect method uses feature rates for prognosis. Based on the positive feedback assumption, as the structure becomes more damaged, the rate of change of the Mahalanobis distance will increase to infinity. In this thesis, the feature rates are found by taking the backwards finite difference between all combination of feature values between adjacent damage levels.

$$R_c = \frac{\Omega_c - \Omega_{c-1}}{t_c - t_{c-1}} \tag{1.22}$$

where:

R_c = The rate of change of the Mahalanbois distance at a given current time t_c

Ω_c = Mahalanbois distance at a given current time t_c

Ω_{c-1} = Mahalanbois distance at a given past time t_{c-1}

1.3.2   Feature Value Method-"Direct"

Another approach to Voights failure forecast method was tested against the data set. Instead of calculating the feature, finding features rates, and finally using linear regression to predict time of failure, the modified model established a direct connection from the feature values to the time of failure predictions.

After setting α to two and $\frac{1}{R_f}$ equal to zero for the general feature solution, we arrive at the final equation for the direct method.

$$t_f = \frac{e^{\kappa * \Omega} * t}{e^{\kappa * \Omega} - e^{\kappa * \Omega_0}} \tag{1.23}$$

If κ is known, time of failure can be solved for directly from the feature values. κ will be solved for by using a nonlinear analysis to best fit the general feature solution to the data.

1.3.3 Damage Prognosis Hypothesis

Model

Both processes were tested and compared against each other to find the best model for damage prognosis. For the rest of the paper, the failure forecast method that involves calculating the feature, finding features rates, and finally using linear regression to predict time of failure will be called the indirect method. The failure forecast method that involves straightforward calculation of time of failure from feature values will be called the direct method. It is hypothesized that the direct failure forecast method will perform better than the indirect method overall. Numerical differentiation of discrete noisy data introduces more noise into the derivative because the effects of the noise are combined in calculating the rate of change. By avoiding the need to calculate the rates in the direct method, the induced noise associated with the derivatives noise can be eliminated. In efforts to produce consistently earlier accurate predictions with higher confidence levels, the differentiation process will be avoided all together. Large noise levels may have serious effects on the prognostics. Because the SHM system uses a data driven approach, the predictions are heavily influenced by the data, and therefore are also impacted by noise. If the noise is too great, the SHM system may return poor, inaccurate, or indiscernible predictions.

Overall Behavior

Generally, predictions that are made that are far from failure should have large standard deviation and peaks that are far from failure. As failure is approached the standard deviations should become smaller and the peaks should converge to the actual observed time of failure.

This progression is desirable and expected. It means that the variance in prognosis predictions decreases with time. As time progresses, the rate-based positive feedback behavior will be revealed. When the panel is healthy, the input data sets should be almost indiscernible from each other. The variation in the peak predictions will then be mainly skewed by any noise and bias, causing the peak predictions to exist within a wide range of values. Only when the feature and feature rate data sets start to noticeably increase exponentially will the prognostics start to stabilize at and gravitate towards the observed time of failure. This circumstance will happens when failure is relatively close. During this time, the increase in feature and feature rate values operates on a larger scale than the noise and bias. The growth in observed values then overcomes the noise and bias and will responds with better predictions.

Predictions

The range of peak predictions will not always situate around the observed time of failure if there are unforeseen biases in the data. Some results may have positive biases and other have negative biases. A positively biased prognosis predicts time of failures that are too high. Bias of this type are incredibly dangerous. Predictions from positively biased features puts the lives of the crew onboard a naval vessel into jeopardy and places national security at risk. A negatively biased prognosis predicts time of failure sooner than what would actually occur. Though they are less dangerous, predictions from negatively biased features can still have serious problems associated with them. Negatively biased predictions are costly when naval vessels are grounded for maintenance or inspections. More importantly, grounding threatens homeland security when the vessel is purposefully removed from active duty.

1.4 Contributions of Thesis Work

The significant contributions of this thesis are summarized as follows:

1. A experimental test is orchestrated to validate the use of fiber optic sensors as a SHM sensing solution within composite materials.

(a) No indication of fatigue damage or wear-out of the sensor array or connections were observed because of the fatigue tests.

(b) Embedded fiber optics were less likely to experience breakage than exposed fiber optics.

2. Positive feedback behavior is cross-examined with fatigue failure.

(a) Increasing feature rates are observed.

(b) Asymptotic behavior is not observed.

3. A rate-based SHM failure forecast method is implemented to ultimately predict time of failure.

(a) The linearized failure forecast method has potential to accurately predict time of failure.

(b) Non-damaging related extraneous factors increase feature variability and decrease prognosis accuracy and precision.

Chapter 2

Experimental Setup

2.1   Introduction

In Chapter 4 the experimental setup used to validate the SHM damage prognosis model is described in greater detail. Firstly, specimen descriptions are provided and details about the test panels are given. Next, the instrumentation, test fixture, sensors arrangement, and mechanical systems are depicted. Finally, the testing protocol is explained.

2.2   Test Specimen Details

2.2.1   Panels

Through a vacuum oven system, eight FRP panel laminates were fabricated for the Phase II test series. Axion AX-3201s/EL woven glass pre-preg fibers and toughened epoxy were cured at 93.3 C to achieve a target thickness representative of a submersible vessel's hull. All were made to be 10 wide, 32 long, and approximately 0.6875 thick.

The eight panels were then divided into two groups of four specimens. For the first round of testing, the fiber optic sensors were bonded to the outside surface using an epoxy adhesive. These panels will be noted as: Panel 1, Panel 2, Panel 3, and Panel 4. The panels in the second round will be called: Panel 5, Panel 6, Panel 7, and Panel 8. Panel 5 and Panel 6 had the same integrated sensor arrangement as the panels used in the first round of testing. Panel 7 and Panel 8 had a different setup. Panel 7 had sensors on both the bottom and the top surface. The top

surface was similar to the sensor arrangements of the first round panels. The bottom surface had a different arrangement. The fiber optic on the bottom surface were instrumented with two 3-D printed sensor housing on each fiber optic cable egress. The entire bottom surface was also covered with an additional epoxy-glass reinforcement cover ply. Panel 8 was instrumented with one fiber optic sensor. The sensor had the same 3-D printed sensor housings and cover ply arrangement as Panel 7 but was instead located on the top surface.

Figure 2.1. Specimens in fixture.

2.2.2 Sensor End Housings

The sensor end enclosures were made from acrylonitrile butadiene styrene (ABS) plastic material. They were designed to make connecting to the data acquisition (DAQ) system easier and to protect the fiber optic ends. The Digital Media Lab at UCSD Geisel Library manufactured the housing using an .4mm diameter nozzle attached to an Ultimaker 3 printer. For the purpose of the Phase II objectives, these choices for material, design, and manufacturing method are permissible. In reality, if a vehicle is manufactured with the proposed SHM system, a more appropriate design should be tested for higher-performance guidelines.
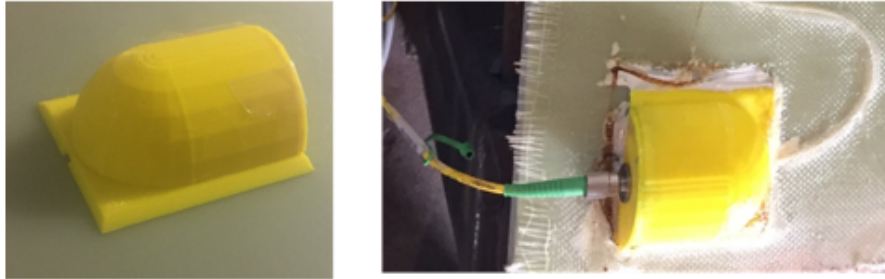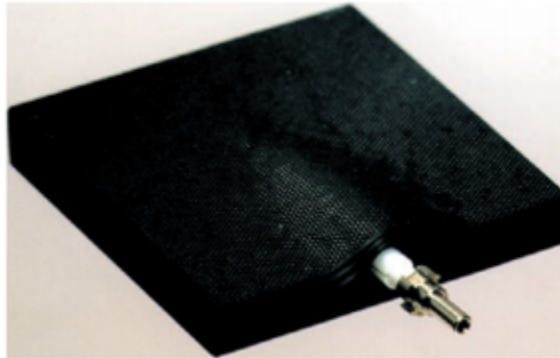
Figure 2.2. Used sensor end housing.

Figure 2.3. Possible sensor end design.

2.3 Test Setup

Testing was conducted at HI-Test Laboratories in Arvonia, Virginia with the help of Applied Physical Sciences. The experimental testing setup goes as follows. A series of shims and bolted connections fixed the edges along the width of the panel onto a tooling fixture attached to a shake table. The shake table served as a mechanism that would induce a dynamic sinusoidal loading onto the panel. This arrangement alone could not produce damage propagating inertial dynamic forces. The self weight of each panel was far too light to significantly create damage from the shake table's dynamic displacements. Equivalently, the rigidity of the panel being tested was far to large to observe large damage generating displacements. As a work around, masses were attached to the top and bottom surfaces of the panel through a system of threaded rods, shims, and bolts. The dummy mass system acted as a means to increase the inertial dynamic applied forces. With the masses, the shake table could operate comfortably to produce damage

propagating strain levels.

Lateral crossbars were added onto the fixture for convenience. The crossbars allowed engineers to quickly assemble and disassemble the masses from the panels during the interim time in between damage propagation and data collection phases. This system was preferred because more cyclic testing periods could be conducted in a short amount of time.

Though lateral crossbars on the fixture permitted easy accessibility to the panels and the masses helped propagate damage, they both created an upper limit on the behavior. Some panels reached a point where the deflections would cause the masses to hit the crossbars. Some panels reached a point where the deflection caused the actual masses to hit each other. Testing of a panel ended and panel failure was defined at point of first contact.
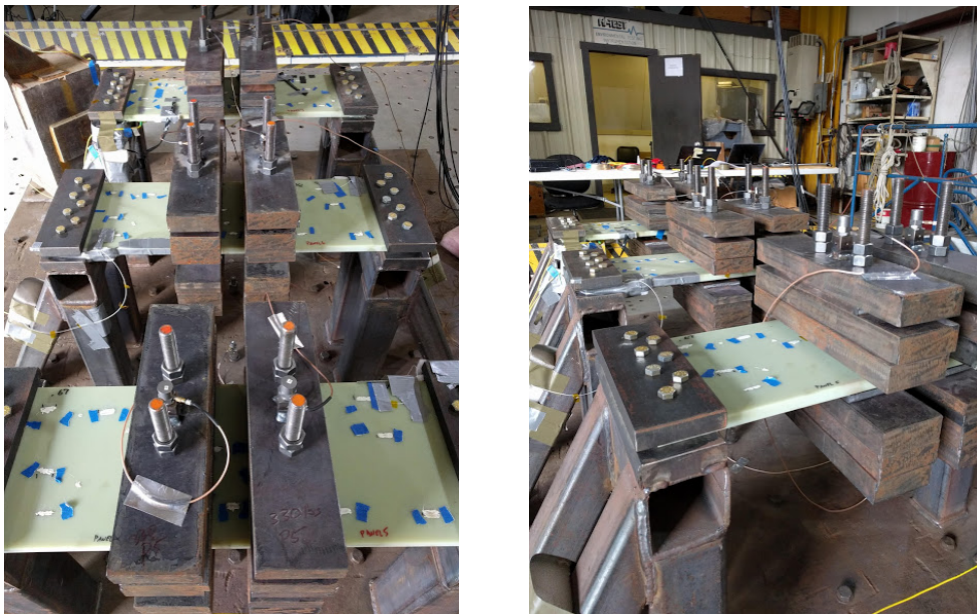

Figure 2.4. Contributors to thesis
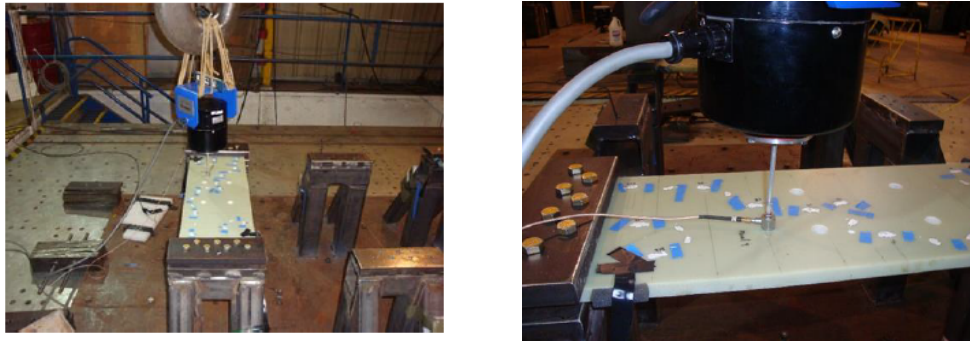

Figure 2.5. Specimens with loaded masses.

Figure 2.6. Modal shaker used to excite structure for data collection.
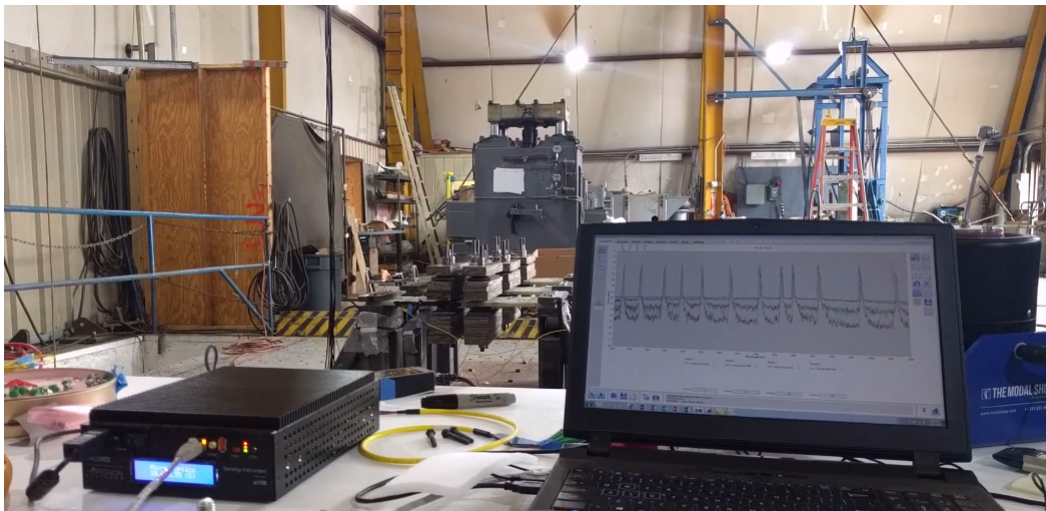
Figure 2.7. View of the test setup.

2.4   Testing Procedure

Prior to any damage levels, visual inspection was conducted and baseline readings for each panel were gathered. A series of data collection instruments were used in the process. A leveled 25 lb. MB Dynamics shaker was hung by bungee cords and attached to the top side of the panel with a plastic stinger. The bungee cords serve to eliminate any spectral coloring of the input from a solid fixture. Powered by an MB Dynamics SL500VCF power amplifier, the modal actuator excited the panel with a BLWN input for two minutes. The excitation signal was generated by a function generator in MATLAB and a National Instruments cDAQ-9178 data acquisition system sent the BLWN output voltage to the power amplifier, and subsequently, to

the shaker. While the panel was being excited, a Micro Optics Hyperion Platform si155 optical interrogator passed broadband light through the fiber optics and recorded the wavelength of the reflected light from each FBG.

Band-limited white noise (BLWN) was the input of choice because it is assumed to represent a pseudorandom operational environment of what would be experienced by a composite in service at sea. It is assumed that the environmental conditions surrounding a naval vessel and the working on-board naval mechanical system superimpose together to provide an ambient excitation on the panel that resembles BLWN. The BLWN input should ideally have the largest frequency range as possible. By exciting the panel with a broadband input, an equally comprehensive dynamic response can be observed. The BLWN excitation had frequency content ranging from 10 to 2500 Hz. These limits were chosen strategically. The lower limit excludes lower frequency content that are of the same order as the suspended shaker's oscillations. Input frequencies less than 10 Hz may excite the entire shaker and cause the input being applied directly to the panel to severely deviate away from BLWN. The upper limit is the Nyquist sampling frequency for the optical interrogator. Because the interrogator samples at 5000 Hz, the highest frequency that can be in the recorded output signal is 2500 Hz. 2500 Hz is an appropriate choice for the input's upper limit because a linear dynamic system will have the same steady state output response frequency as the frequency of the dynamic input. The post-processing chapter will explain how transient dynamic responses are removed to ensure that only the recordings from the steady state behavior are considered.

After the baselines were collected, the dummy masses noted previously were installed onto the panels and the shake table ran to a target damage level cycle count. When the target damage level was reached, the shake table would be shut down, the masses would be removed, inspection would be conducted, and shake tests would be performed again. This cyclic process repeated for each panel until panel failure was reached.
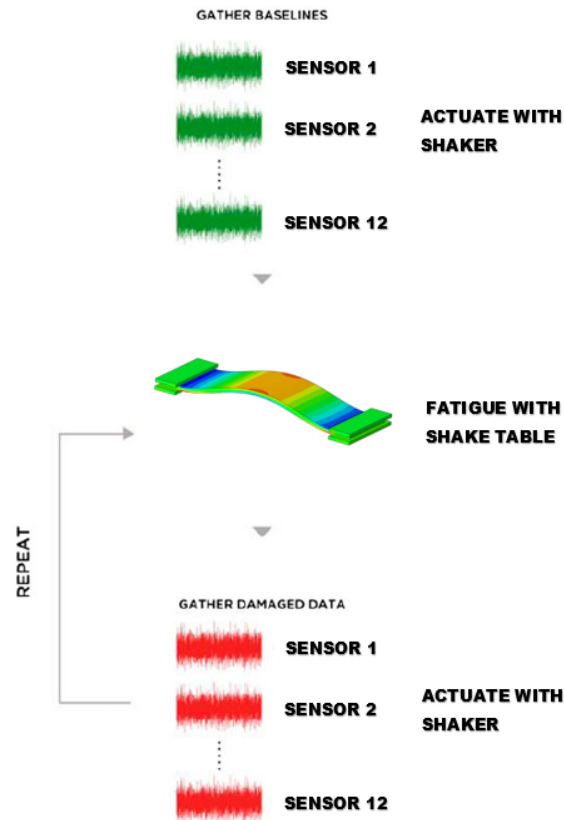
Figure 2.8. Testing flow.[42]

2.4.1 Sensing System Description

The large strains developed during damage phases produced reflected wavelength readings outside of each FBG sensor's designed spectral range; ruling out the possibility of using the fiber optic sensors to monitor each panel during fatigue cycles. To monitor the panel during damage phases, accelerometers were attached to these masses and the base of the test fixture. The relative acceleration between the panels and the table helped indicating damage to the specimens.

The fiber optic sensors used on all the panels were specially manufactured by Alxenses. The diameter of the core and the cladding together were on the order of 125 microns. In the future, because the optic used is on the order of 125 microns in diameter, fully embedding the sensor array into the composite during manufacturing is a likely endeavor.

To determine the optimum FBG sites, a modal analysis on the panel and a finite element strain contour plot were analyzed. The locations of the FBGs were selected to not only capture peak strain to noise ratio values but also be diverse enough to represent the full range of the panels frequency and deflection characteristics. Each grating was oriented parallel to the length of the panel.
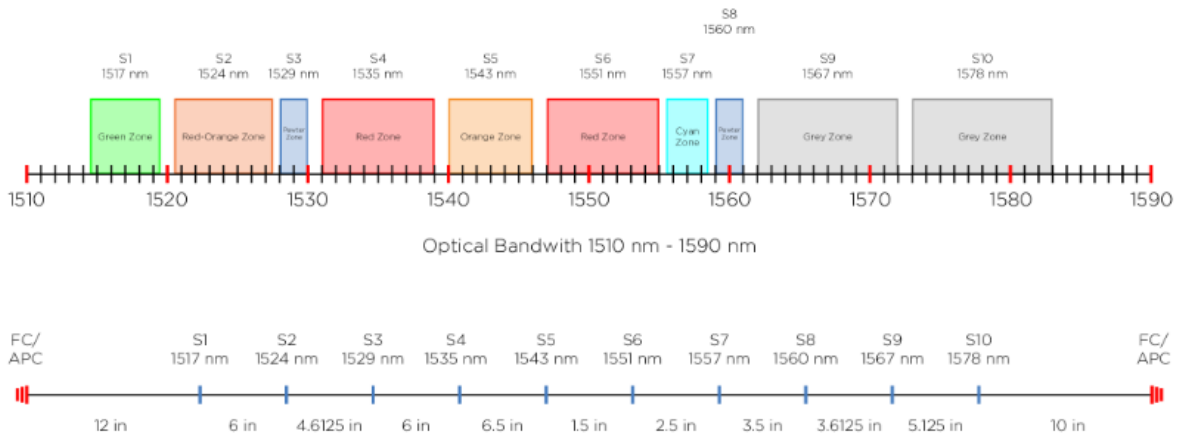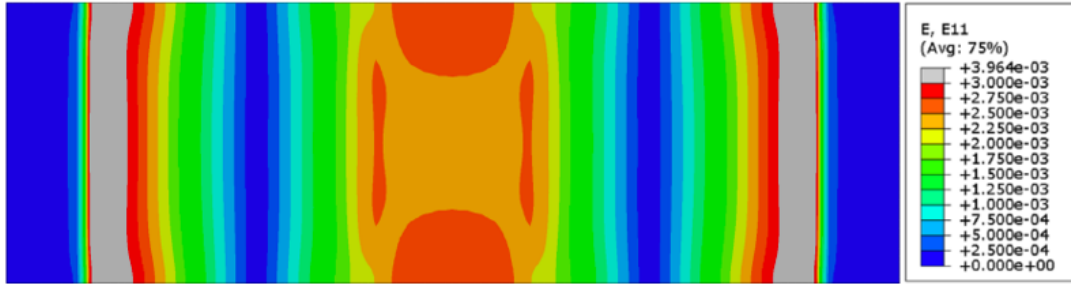

Figure 2.9. Array center wavelengths and dimensions

Sensor	Color	Peak Strain	Proposed center WL (nm)	Lambda (nm)	Delta Lambda (m)	Min Lambda (nm)	Max Lambda (nm)	Envelope (nm)	Envelope Round Up (nm)
S1	Cyan	1.00E-03	1512.0	1513.1803	1.1803	1510.8197	1513.180	2.3606	3
S2	Green	1.75E-03	1517.0	1519.0735	2.0735	1514.9265	1519.074	4.1470708	5
S3	Red-Orange	2.75E-03	1524.0	1527.2760	3.2760	1520.7240	1527.276	6.5520141	7
S4	Pewter	7.50E-04	1529.0	1529.8950	0.8950	1528.1050	1529.895	1.7899771	2
S5	Red	3.00E-03	1535.0	1538.6003	3.6003	1531.3997	1538.600	7.2006495	8
S6	Orange	2.50E-03	1543.0	1546.0147	3.0147	1539.9853	1546.015	6.0294574	7
S7	Red	3.00E-03	1551.0	1554.6379	3.6379	1547.3621	1554.638	7.2757052	8
S8	Cyan	1.00E-03	1557.0	1558.2154	1.2154	1555.7846	1558.215	2.430816	3
S9	Pewter	7.50E-04	1560.0	1560.9131	0.9131	1559.0869	1560.913	1.8262684	2
S10	Grey	4.00E-03	1567.0	1571.9043	4.9043	1562.0957	1571.904	9.8086831	10
S11	Grey	4.00E-03	1578.0	1582.9388	4.9388	1573.0612	1582.939	9.8775379	10
S12	Yellow	2.25E-03	1587.0	1589.7901	2.7901	1584.2099	1589.790	5.5801632	6
TOTAL REQUIRED BANDWIDTH (nm)									71

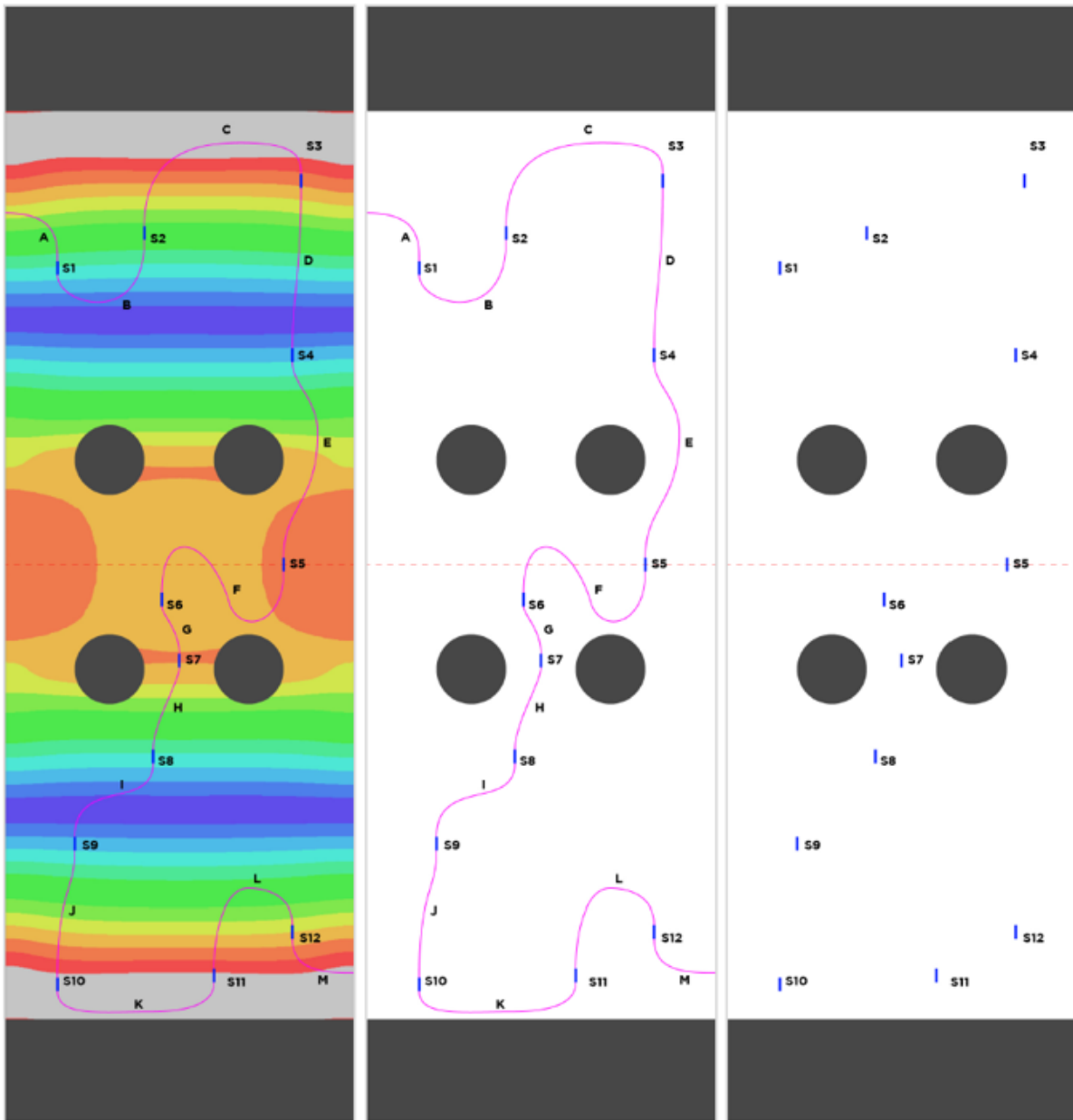**Figure 2.10.** Modal analysis for peak location selection.

Figure 2.11. Array layout.

Chapter 3

Post-Processing

3.1 Introduction

Before any description of the post-processing procedures is given, the testing procedures should be made clear. Below is a list that summarizes the step by step testing procedures:

    I Baseline data is gathered.

    II Masses are loaded onto a panel.

    III Shake table is initiated.

    IV Damage cycle count begins when accelerations stabilize.

    V Damage cycle count stops when target cycle is reached.

    VI Shake table is turned off.

    VII Damaged data is gathered.

Steps II through VII repeat until panel failure. A series of data handling techniques were implemented on the collected data. The transformation procedure from wavelength readings to failure predictions will be described first. Next, the data compression process is discussed. Finally, the statistical model to present the results is specified. The following data transformation and prognosis procedures in this chapter occur every time data was gathered.

48

3.2 Data Transformation

For one data collection instance, the fiber optic interrogator collected twelve wavelength time histories spanning two minutes - one recording at each FBG sensor location. Each wavelength time history was first converted into strain time histories. Then, each full two-minute strain time history was windowed into 60 separate two second time recordings. The first and last two second time records were excluded from the data to account for any transient behavior of the electromechanical shaker. Now 56 strain recordings are left at each FBG sensor location. The 56 separate strain recordings act as if the output strain response was recorded 56 separate times at each of the twelve sensor locations durine a data collection phase. See Figure 3.1 for a visual depiction of the post processing procedure up to this point

The baseline CPSD plots between all different combinations of FBG sensors pair locations are documented first. From the baseline measurements, 56 randomly chosen strain recording pairs were selected for signal processing among the 56 strain recordings at one distinct sensor location and 56 strain records at a different distinct sensor location. 56 CPSD plots were created from the 56 randomly chosen strain recording pairs. All of the 56 baseline CPSD plots between a sensor pair were then compressed into an average CPSD baseline plot. Now, there is one baseline CPSD plot for each sensor pair. See Figure 3.2 for a visual depiction of the post processing procedure described in this paragraph.

Damage in the non-pristine structure produced strain recordings that deviate from the baseline recordings. CPSD plots produced from the non-pristine structures will be referred to as damaged CPSD plots. The same procedure to find the baseline CPSD plots is used to find the damaged CPSD plots. The damaged CPSD plots generated are not compressed into an average CPSD plot like the baselines. Each damaged CPSD plot is cross examined with the single baseline CPSD plot. The resonant frequency locations from the damaged CPSD are found and compared to the natural frequencies of the baseline CPSD plot. Then, the natural frequency perturbations due to damage are assembled into a multidimensional feature of peak shifts and
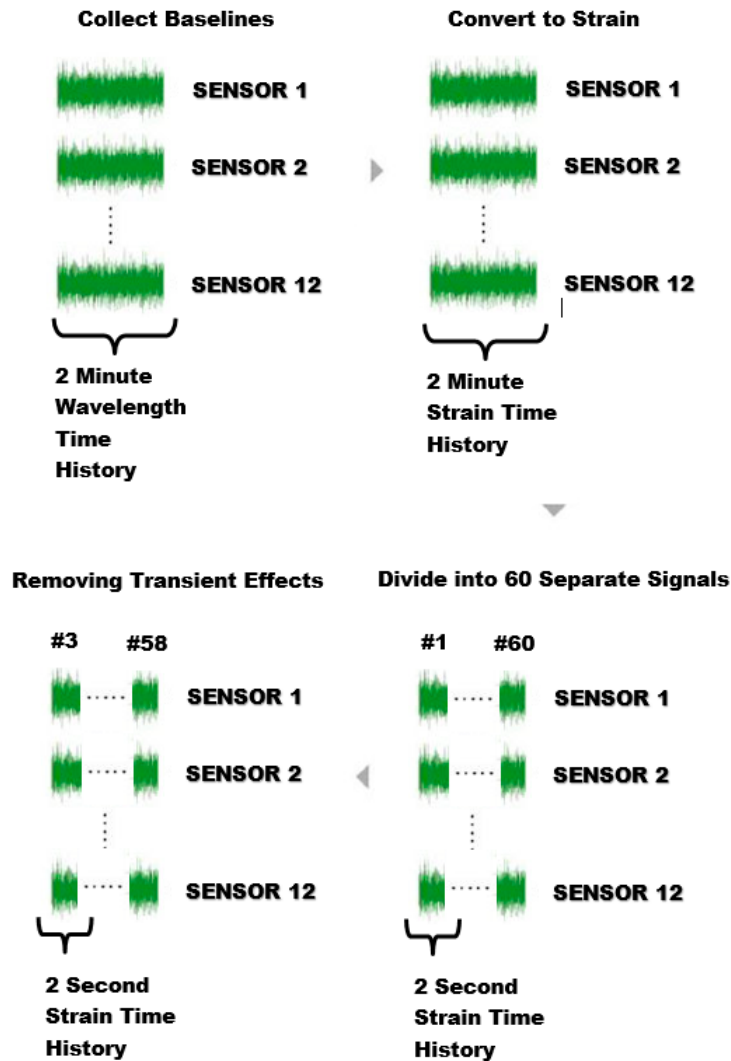
49

Figure 3.1. Data Transformation - Baseline Wavelength signals to separated baseline steady state strain signals.

compressed into the Mahalanobis distance metric. For a given sensor pair, the baseline training set data is used to calculate the covariance matrix. Now for each sensor pair, 56 Mahalanobis distances exist for a particular damage level. The 56 separate Mahalanobis distances for a sensor pair act as if the Mahalanobis distance was recorded 56 separate times at a particular damage level. When another damage level was observed, 56 more Mahalanobis distances were recorded and added the existing sensor pair data set. See Figure 3.3 and Figure 3.4 for a visual depiction of the post processing procedure described in this paragraph.
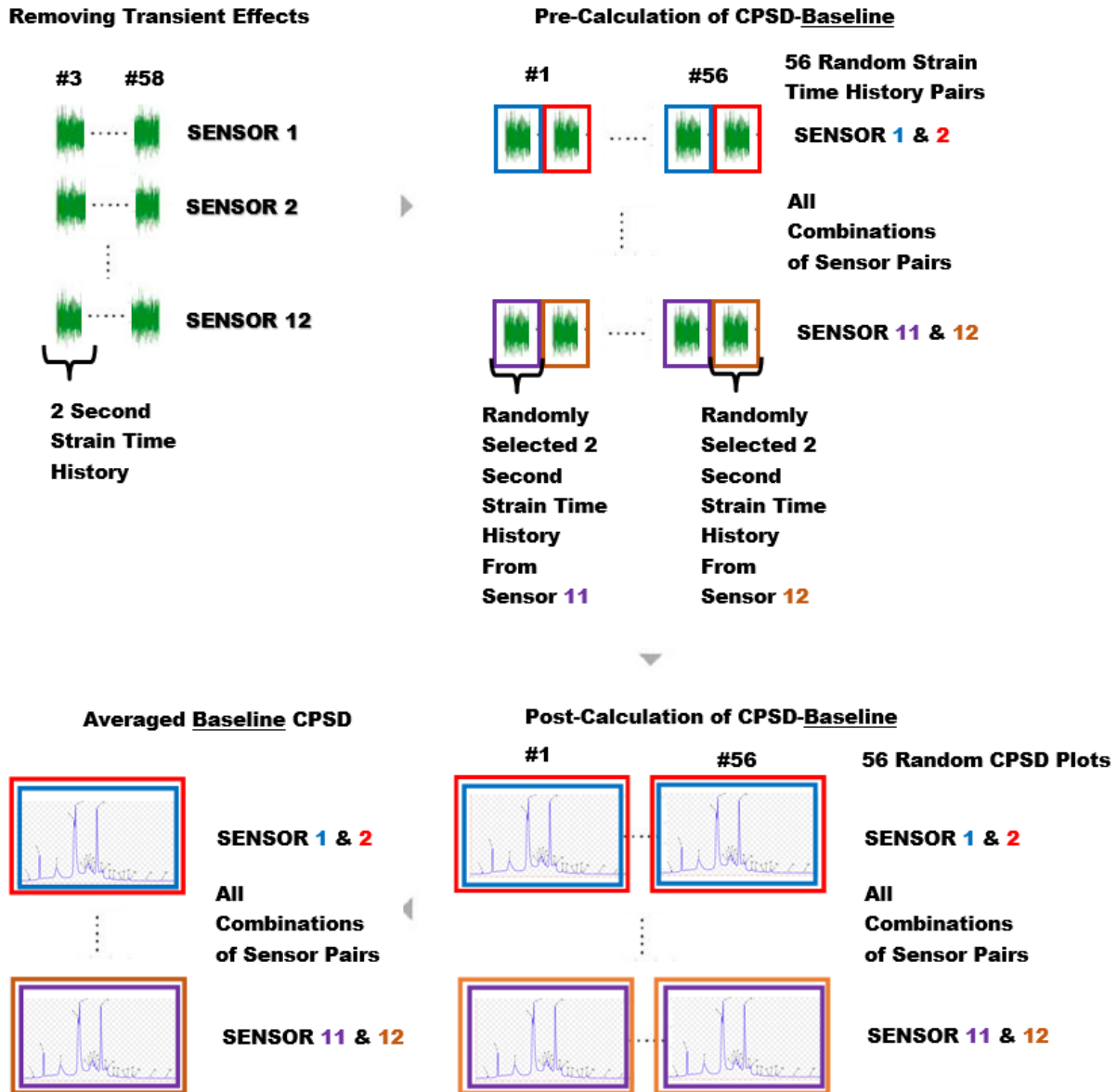
Figure 3.2. Data Transformation - Separated baseline steady state strain signals to Baseline CPSD plot.

To calculate the rate of change of the Mahalanobis distance feature, all combinations of the backwards finite difference was taken between Mahalanobis distances among adjacent damage levels. At a particular damage level for a sensor pair, 3136 Mahalanobis distance feature rate data points now exist. The 3136 Mahalanobis distance feature rate data points act as if the Mahalanobis distance feature rate was documented 3136 times at a particular damage level for a
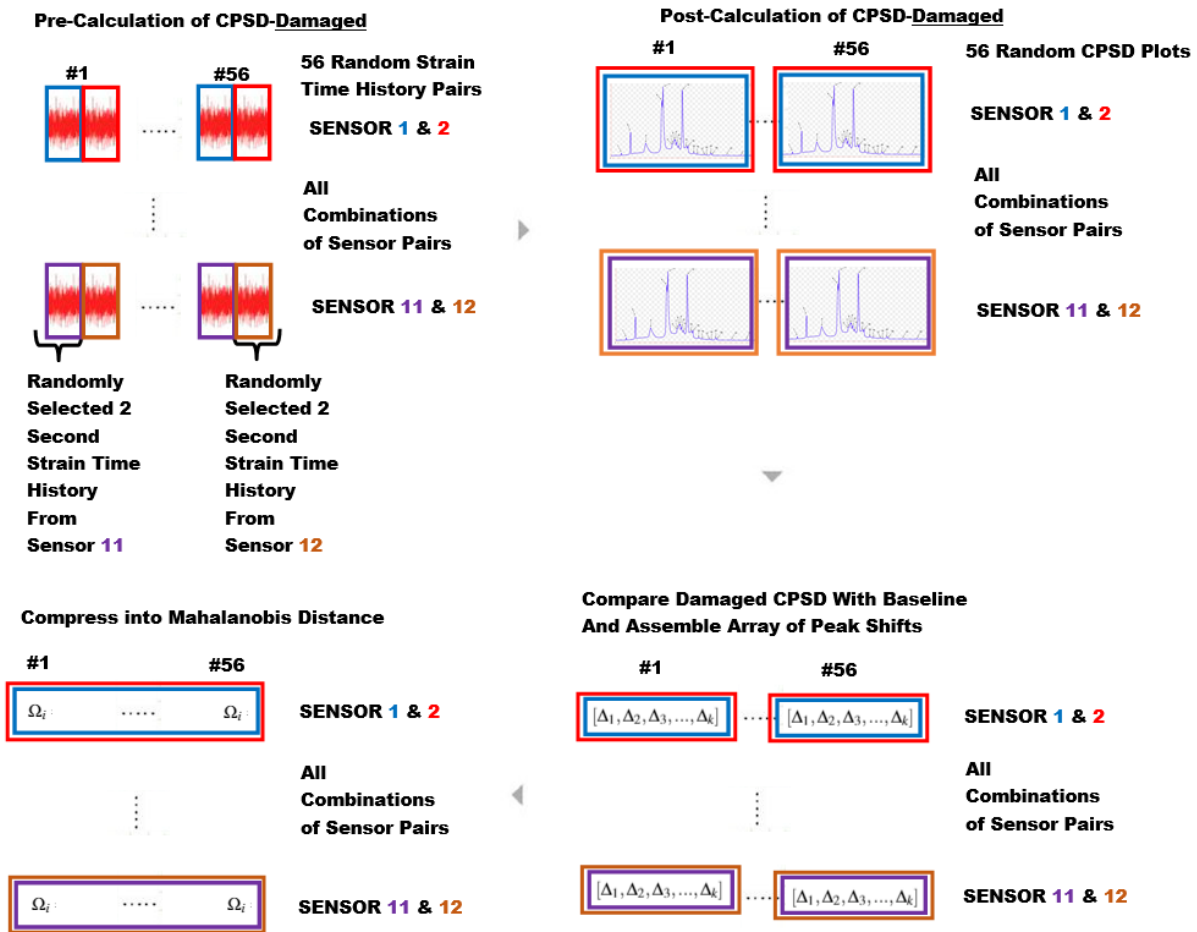
Figure 3.3. Data Transformation - Separated damaged steady state strain signals to Mahalanbois distance.

sensor pair. See Figure 3.4 for a visual depiction of the post processing procedure described in this paragraph.

3.2.1 Indirect Method

The indirect linearized failure forecast method requires at least two observed Mahalanbobis feature rates at two different times to calculate time of failure. All possible combinations of feature rates between two adjacent damage levels would produce 9834496 time of failure predictions. Computing 9834496 predictions for each damage level across all sensor pairs took far to long to be practical for this research. Instead, 3136 random rate pair combinations between
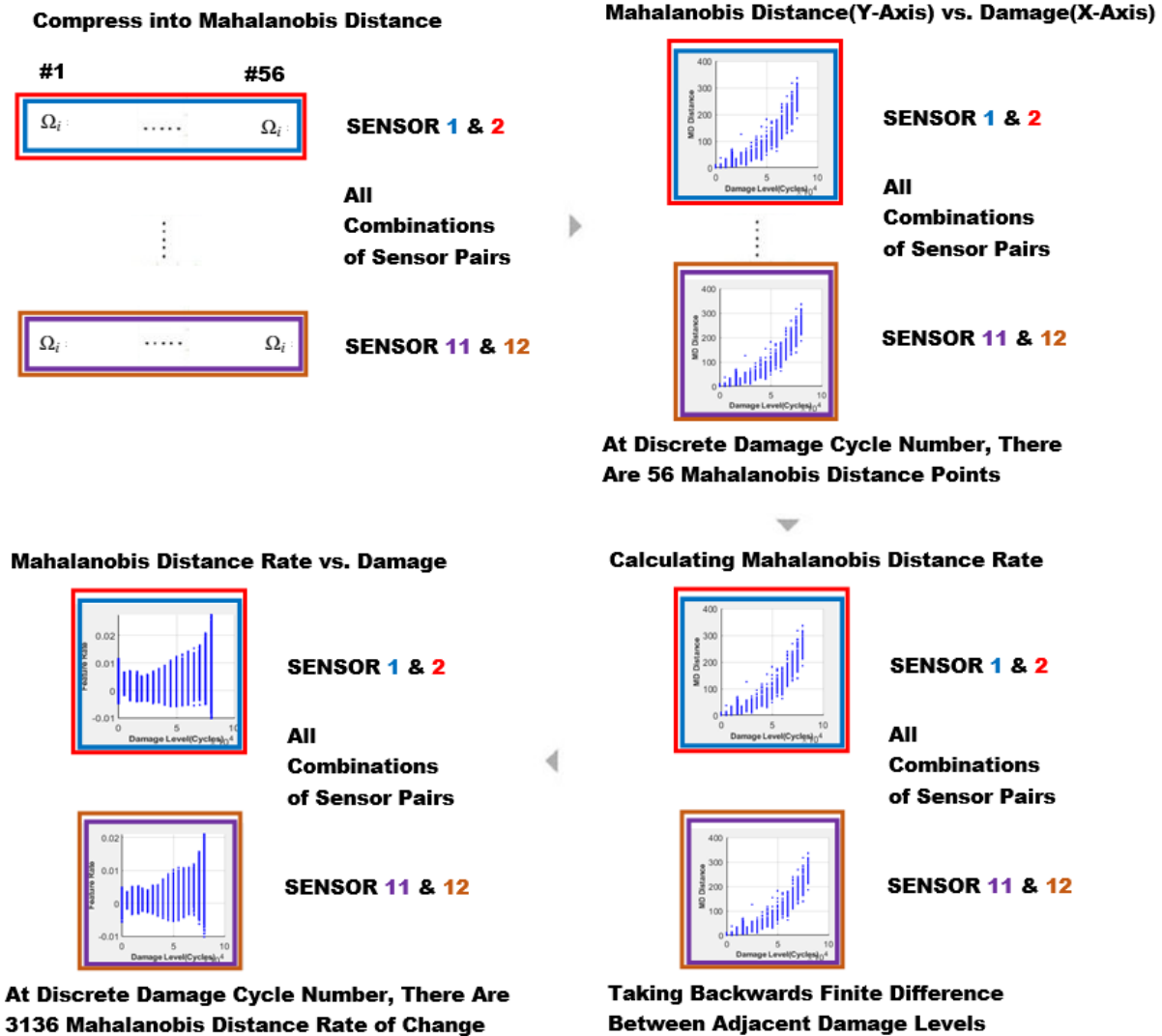
Figure 3.4. Data Transformation - Mahalanobis distance to Mahalanbois distance rate of change.

two adjacent damage levels were selected to be passed through the indirect linear failure forecast method. Negative rates were ignored. See Figure 3.6 for a visual depiction of the post processing procedure described in this paragraph.

3.2.2   Direct Method

The direct method requires a singular feature value to calculate time of failure. For each damage level across all sensor pairs, the 56 feature values will create 56 time of failure predictions. See Figure 3.5 for a visual depiction of the post processing procedure described in

this paragraph.

3.3   Data Compression

3.3.1   Mean Time of Failure Predictions

The direct and indirect method will produce separate sets of time of failure predictions from the feature and feature rates respectively. At each damage level where data was collected, a time of failure prediction data set will exist for all the sensor pairs. Within each sensor pair, time of failure data sets at each damage level will be compressed into an average time of failure prediction. Now, instead of having a distribution of predictions at each damage level, each sensor pair has one mean time of failure prediction at each damage level. See Figure 3.5 and Figure 3.6 for a visual depiction of the post processing procedure described in this paragraph.

3.4   Statistical Model Development

3.4.1   Selected Sensor Pair Candidates

Only data from ten particular sensor pairs will be used for prognosis. The ten mean predictions will come from the ten sensor pairs that display the most damage, i.e. have the largest average Mahalanobis distance. The sensor pair screening process is done to ensure that predictions from the best sensor pair candidates are used in the SHM algorithm. These ten sensor pairs display the most damage and capture the positive feedback mechanisms the best. Sensor pairs that did not indicate damage when damage was present would work against producing accurate time of failure predictions. See Figure 3.5 and Figure 3.6 for a visual depiction of the post processing procedure described in this paragraph.

3.4.2   Probabilistic Prediction

Finally, the ten sensor pairs and their mean predictions at each damage level are placed into a statistical framework. For each of the distinct damage level, the ten mean predictions at

that damage level from the ten sensor pairs are fit into a normal probability density function. The end result of the statistical model is a probabilistic wide-spread prediction in the form of a normal PDF. The time of failure PDF predictions occur after each time data is recorded at each damage level. See Figure 3.5 and Figure 3.6 for a visual depiction of the post processing procedure described in this paragraph.

3.5 Testing, Data Transformation, and Prognosis

With an understanding of the data transformation and prognosis steps, they can be added to the listed steps in the beginning of this chapter. Below is a list that summarizes the step by step testing procedures, data transformation, and prognosis system. Steps IV through XI repeat until panel failure.

    I Baseline data is gathered.

    II Baseline data is transformed.

    III Prognosis is conducted.

    IV Masses are loaded onto a panel.

    V Shake table is initiated.

    VI Damage cycle count begins when accelerations stabilize.

    VII Damage cycle count stops when target cycle is reached.

    VIII Shake table is turned off.

    IX Damaged data is gathered.

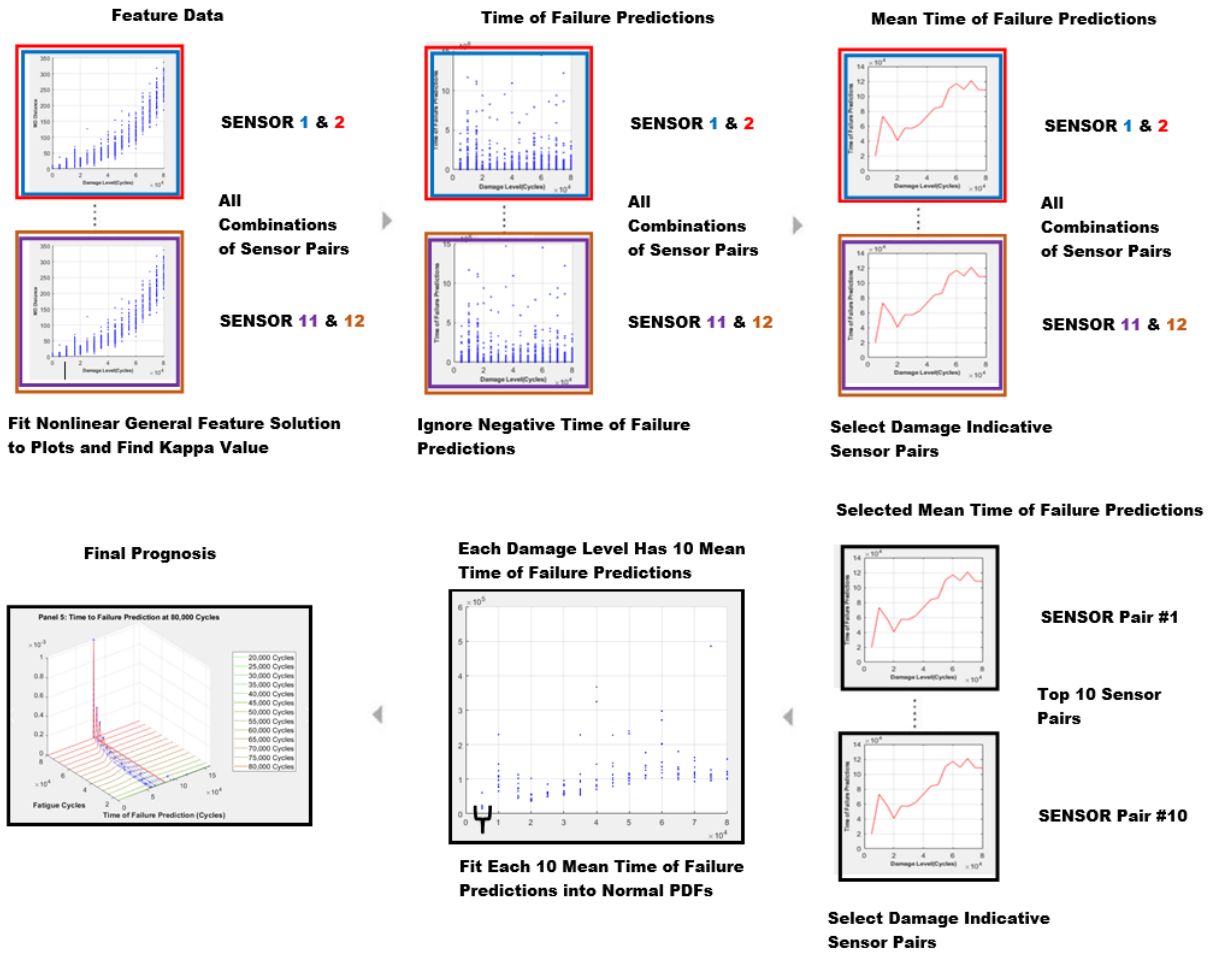   X Damaged data is transformed.

    XI Prognosis is conducted.

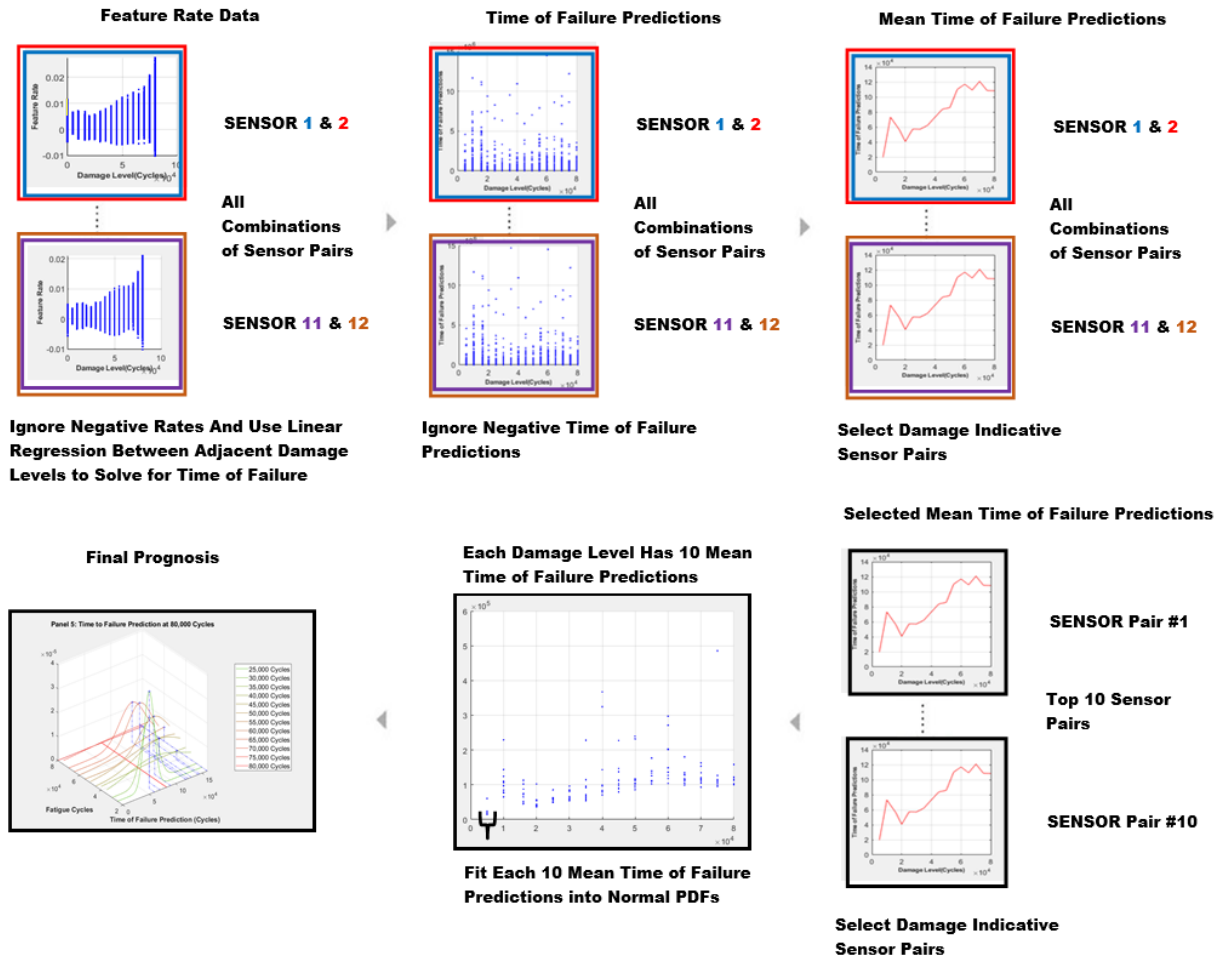**Figure 3.5.** Data Transformation (Direct Method) - Mahalanobis distance to final prognosis

Figure 3.6. Data Transformation (Indirect Method) - Mahalanobis distance to final prognosis

Table 3.1. Sensor Pairs Selected - Panel 5

	Mean Mahalanobis Distance	Kappa (κ)	Alpha (α)
Sensor Pair 3 and 8	72.168	0.03051	2.2082
Sensor Pair 1 and 3	54.793	0.030518	2.1453
Sensor Pair 1 and 8	54.687	0.022723	2.0918
Sensor Pair 7 and 8	54.565	0.046795	2.2265
Sensor Pair 3 and 5	54.233	0.029377	2.1362
Sensor Pair 5 and 8	53.699	0.027801	2.1255
Sensor Pair 3 and 7	51.676	0.046832	2.2102
Sensor Pair 8 and 9	47.771	0.047896	2.2006
Sensor Pair 1 and 5	39.843	0.030662	2.0805
Sensor Pair 3 and 9	38.707	0.09364	2.2699

Table 3.2. Sensor Pairs Selected - Panel 7

	Mean Mahalanobis Distance	Kappa (κ)	Alpha (α)
Sensor Pair 6 and 8	58.588	0.017549	2.0074
Sensor Pair 1 and 6	51.709	0.012566	1.9460
Sensor Pair 1 and 8	50.452	0.0096441	1.8973
Sensor Pair 1 and 4	46.958	0.0098839	1.8966
Sensor Pair 5 and 8	46.604	0.011626	1.9211
Sensor Pair 5 and 6	46.101	0.010056	1.9021
Sensor Pair 1 and 5	45.820	0.013465	1.9367
Sensor Pair 6 and 7	45.272	0.028475	2.0346
Sensor Pair 1 and 2	43.553	0.011434	1.9107
Sensor Pair 2 and 5	42.425	0.012364	1.9192

Chapter 4

Observations and Results

4.1 Introduction

In a real life application of this SHM system, a single prognostic decision would need to be made so that immediate action can be taken from informed decisions. The ultimate goal should be to have the SHM algorithm automatically make this decision within a defined statistical framework, however this capability is not a part of the existing SHM system.

Here we developed the prognosis mechanisms and validated their effectiveness. For now, we can use our engineering judgment to assess how a technician or an automated decision-making process may evaluate time of failure. Furthermore, only the results from Panel 5 and Panel 7 will be discussed. Their prognostics alone capture different types of behavioral trends. Results from both panels also have easily visible cues that will later lead to important topics of discussion.

The experimental arrangement held up throughout the entirety of the scheduled testing duration and all panels were tested to their limits. This chapter comments on notable observations made during testing and post-processing. Then the indirect and direct method results for Panel 5 and Panel 7 are presented and interpreted.

Fiber damage through the
thickness at connection

Delamination at the boundary

Figure 4.1. Panel 5 failed panel.

Fiber and delamination at the
dummy mass connection

Delamination at the connection

Through thickness damage
at the boundary
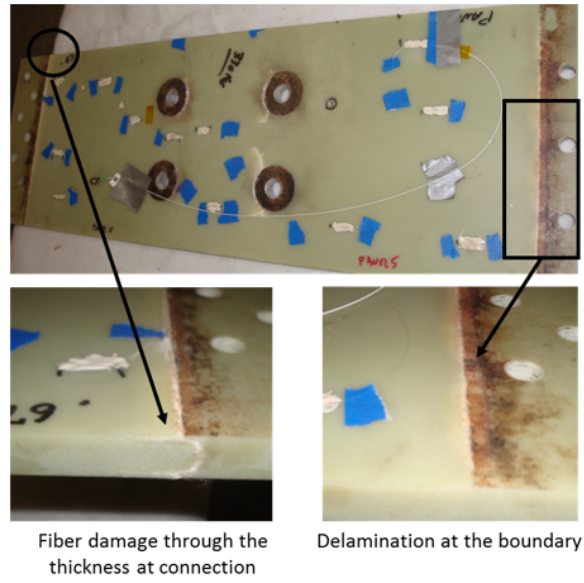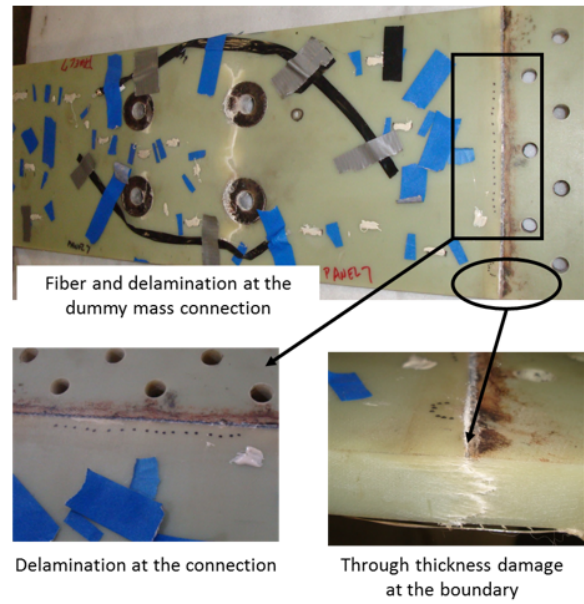
Figure 4.2. Panel 7 failed panel.

4.2 Observations

4.2.1 Damage

Panel 5 and Panel 7 both saw matrix cracking, delamination, bolt bearing damage, crack formation, crack propagation, and boundary condition weakening. Though the panels were identical, they failed at different times. Panel 5 failed at 83000 cycles and Panel 7 failed at 683000 cycles. It is interesting to note that Panel 5 failed sooner than Panel 7 when Panel 7 faced larger inertial dynamic loads than Panel 5. Panel 5 was instrumented with 330 lbs during fatigue phases and was predicted to see strain levels up to 3500 microstrain. Panel 7 was instrumented was instrumented with 345 lbs and was predicted to see strain levels up to 4000 microstrain. The failure of the panel to behave inline with engineer judgment is a prime example of composite behavior complexity and unpredictability, and this inconsistency necessitates SHM because engineering judgment alone cannot guarantee safe use of such multiconstituent material systems.

4.2.2 Sensor Arrangement

None of the fiber optic sensors completely failed because of the fatigue testing regimen. Meaningful data was collected from each panel. Occasionally, something would mistakenly come in contact with a fiber optic sensor, breaking a sensor in two. Fortunately, the sensor could be salvaged by connecting each end to the interrogator. Panels with the cover ply never experienced fiber optic breakage even when something mistakenly fell onto the sensor. The cover ply acted as an extra layer of protection over the fiber optic cladding which served to prevent the fiber optic sensor from breaking.

4.2.3 Testing Arrangement

Crossbars

Lateral crossbars were added onto the fixture for convenience. The crossbars allowed engineers to quickly assemble and disassemble the masses from the panels during the interim
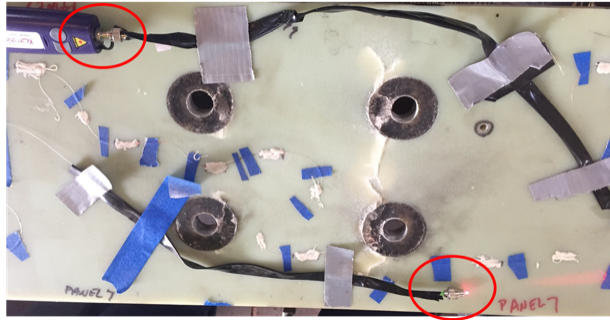
Figure 4.3. End of Test Array Check Panel7.

time in between damage propagation and data collection phases. This system was preferred because more cyclic testing periods could be conducted in a short amount of time.

Though lateral crossbars on the fixture permitted easy accessibility to the panels and the masses helped propagate damage, they both created an upper limit on the behavior. Some panels reached a point where the deflections would cause the masses to hit the crossbars. Equally, some panels reached a point where the deflection caused the actual masses to hit each other. Testing of a panel stopped when any form of contact was made. One could expect that the premature stoppage would bias the prognostics and consistently produce non-conservative predictions; but the early stoppage did not demonstrate that the SHM system could not be used to forecast the early defined time of failure. Conservative and non-conservative predictions were observed.

Loading

The shake table could not immediately start at the prescribed damage propagating load case. To reach the damage propagating threshold, the shake table would need to slowly start up. It was assumed that below the acceleration threshold, the inertial forces would not produce damage. Damage cycles were only counted after the acceleration readings on the panel cross a certain bottom threshold during damage phases. Once a target number of damage cycles was reached, the shake table would slowly decay to rest. The transient effects of the shake table starting up and shutting down theoretically added more damage into the panel than what was actually counted. One could expect that the under-predicted damage levels would bias the results

62

and consistently produce conservative predictions; but the transient effects did not show to impact prognosis. Conservative and non-conservative prognosis was observed.

4.2.4   Damage Level Increments

Panels that experienced smaller damage level increments relative to the final time of failure had better results. Relatively short damage propagation phases directly produced more opportunities where the panel's health could be characterized. With more damage detection instances, damage prognosis can also happen more frequently.

Smaller damage level increments also produced more accurate results. The finite difference between closely spaced damaged levels resembled that of what would be the instantaneous feature rate. Feeding improved feature rate estimates into the model constructed better predictions. Panels that used rate estimates calculated from largely spaced intervals had poor results. In the event of implementing such a SHM system for structural assessment, the effects of sparse data sets could ultimately be avoided by monitoring feature rates in real-time or in short time intervals. Results from Panel 7 are the best example of this phenomenon. Panel 7 contained the largest number of damage levels in its lifetime.

4.2.5   Variability in Features and Feature Rates

The prognostics of the indirect method and the direct method are heavily dependent on the rate and feature data respectively. Figure 4.4 and Figure 4.5 shows an example of the feature and feature rate scatter plots of the best sensor pair candidate for Panel 5 and Panel 7. The top row of each figure are graphs of the observed feature values plotted against the damage level. The bottom rows are graphs of the calculated feature rates plotted against the damage level. The graphs in the left column are shown in a manner in which the gradient from green to red represents the structural health transitioning from its original undamaged state to its failure point. The graphs on the right show the feature and feature rate values at each damage level in blue. Each damage level is then connected by a red line, that connects the mean value at each

particular level.

Noise

Clearly, both the feature data and feature rates have increasing local noise levels as the health degrades. The scatter of feature values and feature rate values are wider at greater damage levels. Though the feature graphs have distinguishable domains at discrete damage levels, the feature rate graphs do not have localized values at a particular damage level. The variability in the rates is larger than the variability of the feature values. The wider rate distributions can be attributed to the rate calculation. By taking the backward finite difference between two noisy feature data sets, the noise is amplified in the feature rates. Large noise levels may have serious effects on the prognostics. Because the SHM system uses a data driven approach, the predictions are heavily influenced by the data, and therefore are also impacted by noise. If the noise is too great, the SHM system may return poor, inaccurate, or indiscernible predictions.
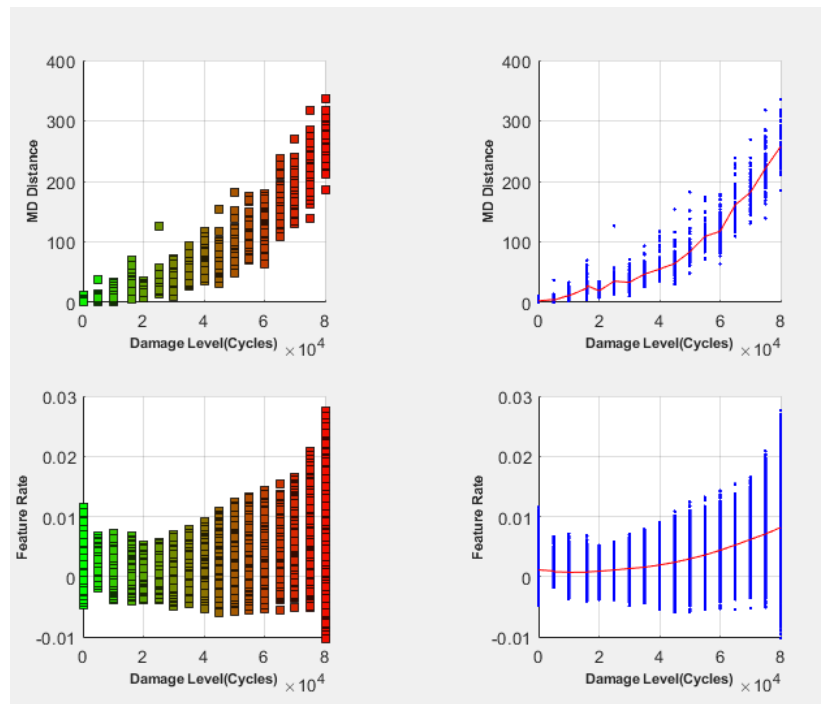

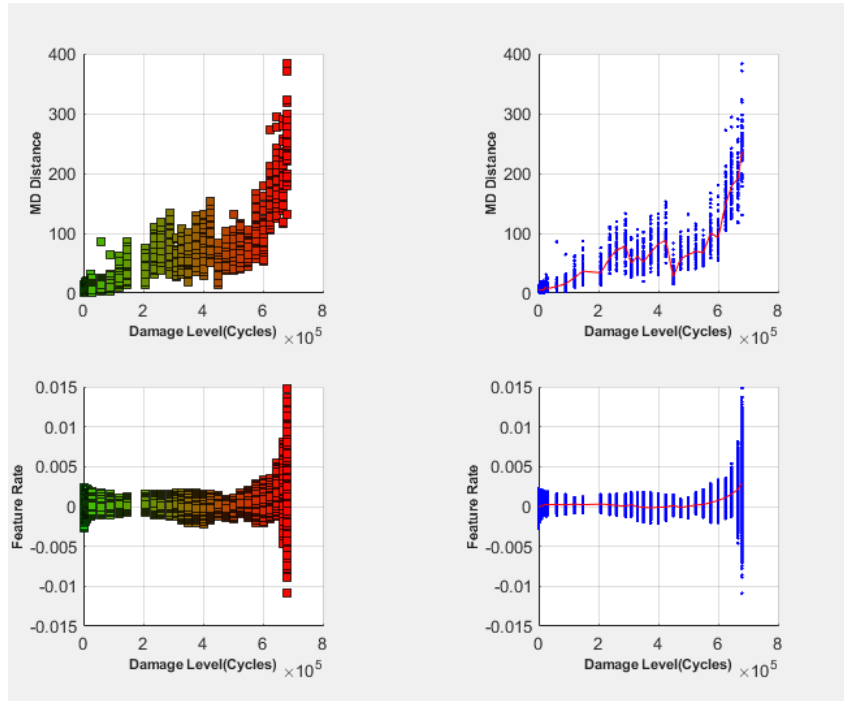**Figure 4.4.** Feature and feature fate values for Panel 5.

Figure 4.5. Feature and feature rate values for Panel 7.

Global Bias

There appears to be an unknown global noise bias alongside the transient local noise levels within the feature values. This behaviour can be seen in the red line connecting the mean feature values at each damage level in Figure 4.4 and Figure 4.5. Panel 7's mean feature line is not as smooth and predictable as that of Panel 5's. Some unknown extraneous factor appears to decrease the feature value. A decrease in the Mahalanobis distance and a negative Mahalanobis distance rate of change would indicate a increase in stiffness and a self-healing panel.

An inconsistent bias could exist on Panel 7. Even a unobvious uniform bias could exist on Panel 5. Bias in the feature values can impact the direct method that involves using the feature values to directly calculate the failure predictions. If the feature values are biased by noise, it is likely that the predictions will also be biased.

65

Asymptotic Behavior

One would think that the global noise bias in the feature rates would be larger because the rates are ultimately calculated from the feature values through the finite difference. This relationship is not the case. The mean rate values behave smoothly, and therefore can work in favor of the prognostics to produce better predictions. Increasing rates are observed overall as damage propagates, but they do not approach infinity, and therefore, do not follow the positive feedback model. Unfortunately, the mean line of feature rates brings into light another predicament; the data does not display the asymptotic behaviour which is an underlying assumption for the positive feedback model. This boundary condition was applied in the beginning of the general model and carries through the entire solution and simplifying assumptions. To that end, panel failure predictions may never refine to the observed time of failure because the observed time of failure may or may not be where the asymptote would truly exist. The data may be essentially represent a different boundary value problem in which the rate at failure has some finite value. One could expect that the misrepresented positive feedback behavior would bias the results and consistently produce non-conservative predictions; but the failure to show asymptotic behavior close to failure did not show to impact prognosis. Conservative and non-conservative predictions were observed.

4.3   Plot Interpretation

The final three dimensional (3-D) plots represent the probabilistic data driven prognosis predictions as a function of damage level. In terms of cycles, the left axis tracks the time at which SHM prognosis was conducted. The right axis provides the time-of-failure PDF prognosis estimates as a function of cycles. At a given amount of endured cycles, each coloured PDF represents the likelihood of time of failure predictions made at a point in time. A final holistic informed decision can be made by considering the PDFs of all SHM prognosis events leading up to the current time.

The two-dimensional plot is a top dead centre view of the 3-D plot such that the origin of the plot is in the bottom right hand corner. The blue crosses mark the peaks of each PDF. The blue lines connect the peaks of the PDFs to their respective time of failure prediction values. The dotted connections help to pin point the most probable time of failure prediction at each prognosis event. The red line represents the actual time of failure.

4.4   Panel 5 - Indirect Method Results

Panel 5 has inconclusive results from the indirect method. The predictions occupy a large range of possibilities and don't show any signs of observed time of failure convergence. The results generally produce non-conservative predictions as well.

Smaller damage level increments may improve prognostics. With the large damage propagation interval used on Panel 5, the estimated rates may be far from what would be the instantaneous feature rate. Misrepresentative feature rate data may have lead to indiscernible results. Furthermore, because the backward finite difference is used to calculate the rates, it is safe to say that the calculated rate would be less than what would actually be observed. The underestimated rates therefore return predictions that will be consistently be positively biased and create non-conservative predictions.

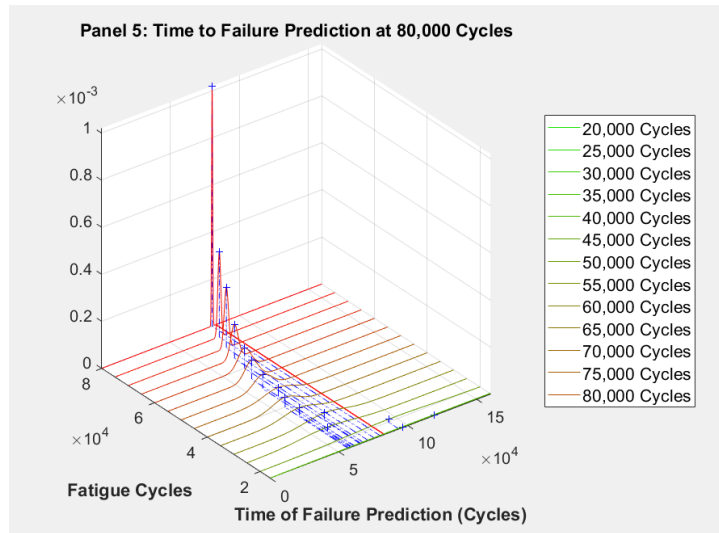**Panel 5 Direct Method Plots (Mean)**

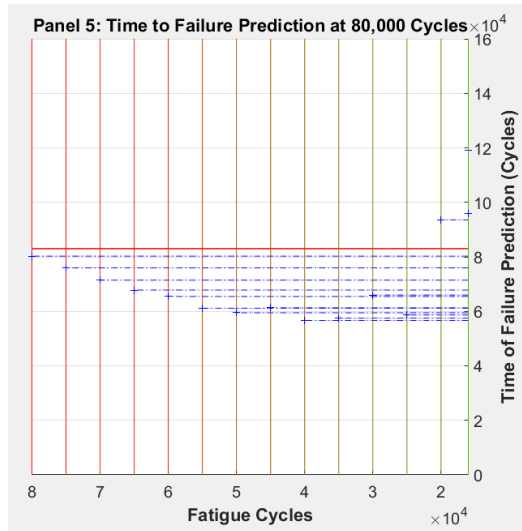**Figure 4.6.** Prognosis evolution plot for Panel 5 (Direct-Mean).

Figure 4.7. Prognosis evolution plot(Top View) for Panel 5 (Direct-Mean).

4.5   Panel 5 - Direct Method Results

Panel 5 has conclusive results from the direct method. At the panel's infancy, the SHM system predicts that the panel is likely to fail within a small range of values around 60,000 cycles. Each PDF leading up to this damage level converges and narrows on this prediction. Once the panel endured 60,000 cycles, each prediction after alerts us that failure is imminent.

Though the results produced a conservative prediction, SHM prognosis was successful and an informed decision could be made with these results. If this panel and method was used in real life, a naval officer may take the submersible vessel offline close to 60,000 cycles to inspect the panel. Upon inspection, the naval office may deem the panel to be healthy and therefore decide to continue to use the panel. The naval officer would then receive repeated and increased warnings that failure is approaching at each prognosis event past 60,000 cycles. He would not only observe time of failure predictions that are repetitively in the near future but also see the probability of these same predictions increasing in value. He then may decide to replace the panel when the probability of failure reaches a certain threshold.

It is interesting to note here that the indirect method returns non-conservative predictions and the direct method produced conservative predictions. One can suggest that the shift occurs when the finite backwards difference is taken between incredibly large damage intervals to estimate the feature rates. Though the feature values originally makes conservative predictions, the severely underestimated calculated feature rates make non-conservative predictions. This comparison reinforces the idea mentioned in the previous section that taking smaller damage increments can create rate estimates that are closer to their true values. Improvements on rate data may then help to increase prognosis accuracy by find a balance between conservative and non-conservative predictions.
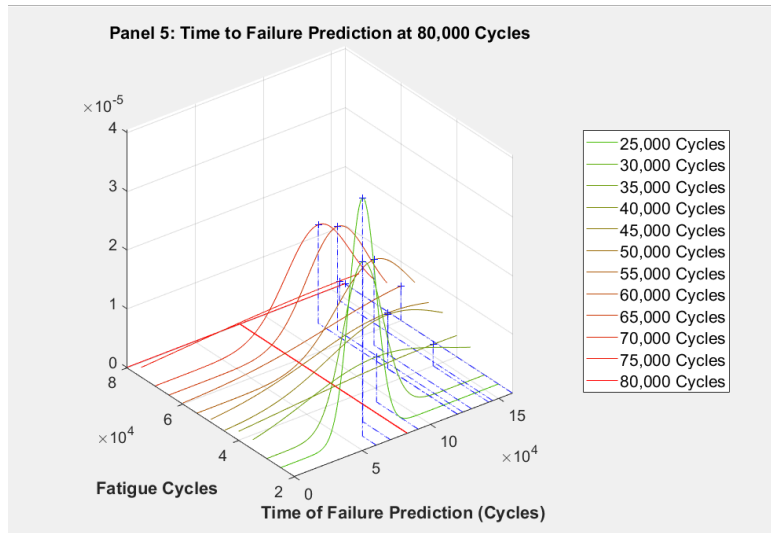
Panel 5 Indirect Method Plots (Mean)

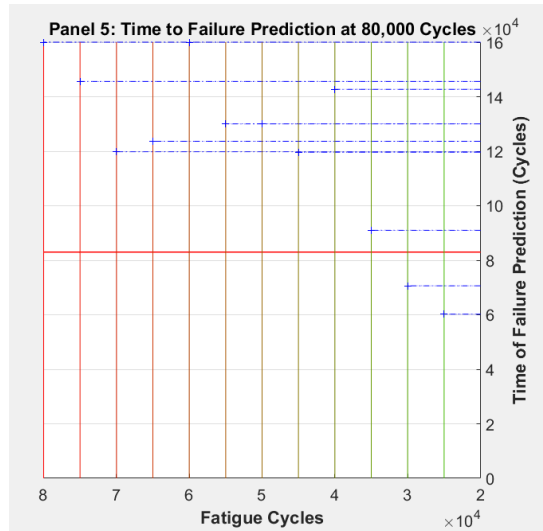**Figure 4.8.** Prognosis evolution plot for Panel 5 (Indirect-Mean).

Figure 4.9. Prognosis evolution plot(Top View) for Panel 5 (Indirect-Mean).

4.6 Panel 7 - Indirect Method Results

The indirect method results from Panel 7 are also conclusive. The predictions are slightly biased. They predominantly have conservative prediction, but the predictions encircle the observed time of failure well. Bias can be assumed to be negligible here. Although the prognosis range is moderately wide, only the poor beginning predictions contribute to the range width. Convergence begins to take effect when the panel has endured half of its total damage capacity and continues to converge until failure is reached.

An automated decision making process may simply disregard the beginning predictions if it is assumed that all beginning predictions have a low probability of being accurate. By doing so, the prognosis range would decrease making the prognosis more accurate overall.

As a reminder, the indirect method uses the feature rate data set for prognostics. In Figure 4.5, the feature rates continuously increase overall. When the panel is healthy, the feature rate values are almost indiscernible from each other. The variation in the peak predictions are then mainly skewed by the noise and not by the observed rates, causing the peak predictions to exist within a range of values. Only when the rates start to noticeably increase do the prognostics start to approach the observed time of failure. The increased rate behavior overcomes the local noise in the rates, and therefore produces better predictions at these levels.
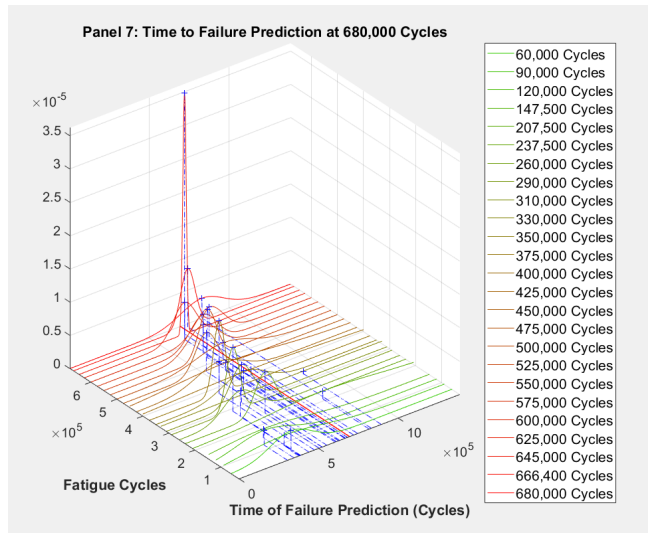
Panel 7 Indirect Method Plots (Mean)

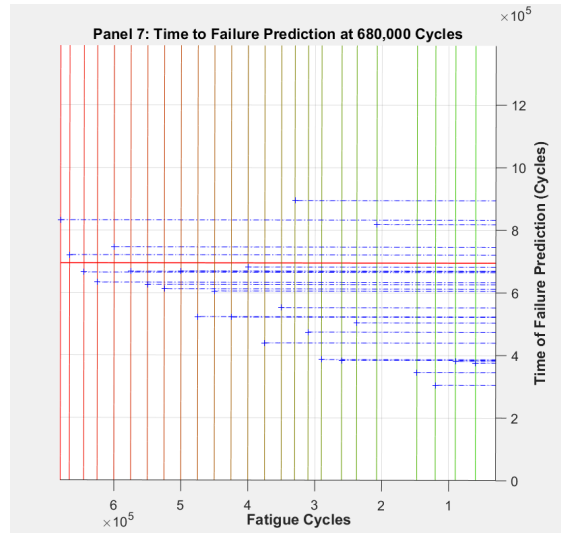**Figure 4.10.** Prognosis evolution plot for Panel 7(Indirect-Mean).

Figure 4.11. Prognosis evolution plot(Top View) for Panel 7(Indirect-Mean).

4.7   Panel 7 - Direct Method Results

The direct method results from Panel 7 are less conclusive from that of the indirect method. the range of predictions is large and there is a positive bias. Convergence is not observed early and culminates shortly before failure.

A more intricate prognosis interpretation process is required here. Each SHM prognosis PDF may need to be weighed differently depending on a number of factors. Some factors include examination time and variance. Prognostics conducted at early stages may be given less weight due to their low probability of being correct. Later predictions can be given more weight as the positive feedback behavior becomes clearer in the data. Equally, highly probable predictions with small variances can be given more weight than predictions with large variances that are unlikely to transpire. Depending on observed data trends and increased pooled data, the weights can self correct to refine the predictions with each prognosis test performed.

The direct method predictions follow the feature data set closely. Though Figure 4.5 shows that each damage level has local distinguishable feature values, there is an obvious unpredictable bias on top of the local noise levels. The noise and bias influences the peak predictions to exist within a wide range of possibilities. Biased feature values return biased predictions leading to peak locations away from the observed time of failure. Noise levels on the feature values alter the variance of each PDF. In Figure 4.12, there are regions where there are moderately narrow time of failure PDFs situated far away from the observed time of failure. These predictions must have had small noise levels but large biases. This behavior is undesired because it would mistaken show moderately large confidence levels supporting an incorrect failure time. When the feature values begin to drastically increase only then do the predictions converge to the observed time of failure. This behavior occurs when the changes in the overall feature values in between damage detection phases dominate over the local noise levels and global noise bias. Perhaps if the global noise bias did not exist, the results of the direct method would resemble that of the indirect method, if not better.

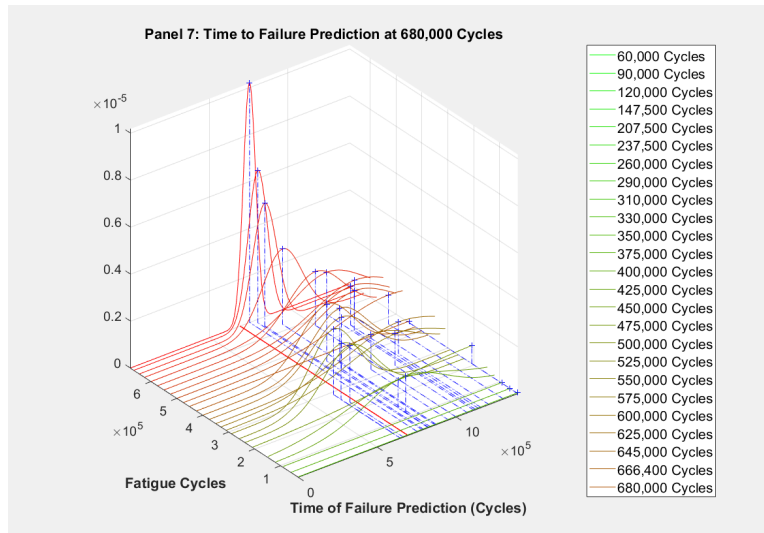**Panel 7 Direct Method Plots (Mean)**

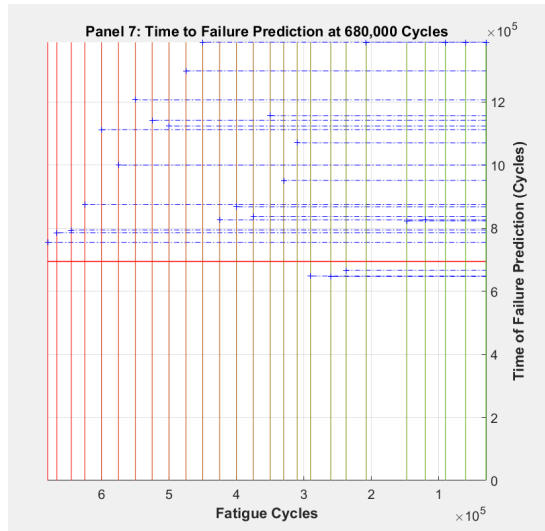**Figure 4.12.** Prognosis evolution plot for Panel 7(Direct-Mean).

Figure 4.13. Prognosis evolution plot(Top View) for Panel 7(Direct-Mean).

Chapter 5

Conclusion and Future Work

5.1   Introduction

Though the results did display promising signs for the positive feedback failure forecast model, the SHM system developed so far is not ready for integration onto any naval vessel. In all cases, the prediction ranges were far too wide to be deemed safe. On some occasions, the time it took for the failure forecast method to provide conclusive results was far too long. Some methods returned dangerous non-conservative prognostics.

This chapter will go on to explain efforts made to improve the results of the mid-scale fatigue tests and point out possible sources of variability within the testing regimen. The chapter will end with possible extensions to the SHM system and concluding statement about the thesis work.

5.2   Corrective Measures

5.2.1   Median Predictions

The statistical data driven prognosis approach used compresses a sensor pairs time of failure predictions into one mean time of failure prediction at each damaged level. Let us examine the results if the median time of failure prediction was chosen instead.

Figures A.1, A.2, A.3, A.4, A.5, A.6, A.7, and A.8 in the Appendix shows the prognostics plots when the median time of failure prediction is used instead of the mean prediction. The

median predictions are consistently sooner than the mean time of failure predictions. Because the predictions are calculated from the feature values and the feature rates, it is safe to say that the feature values and feature rates also have median values that are consistently larger than the mean feature and and feature rate values.

It is unsure why the features do not have the similar or close in value mean and median values. Because the feature data sets have distributions where the mean and median values are not inline, so will the feature rates.

5.2.2   Filters

Digital Filters

All results presented were pre-processed with a digital filter in attempts to decrease the local noise levels and global noise bias. The Savitsky-Golay filter did smooth the recorded data to match the positive feedback assumptions better, but the remaining noise, variation, and bias still produced weak results. When compared to the unfiltered results, the range of predictions did decrease, the distributions narrowed, and the predictions moved closer to the observed time of failure, but not to the extent where the prognostics could be considered to be accurate, precise, and safe.

This filtering method did somewhat distort the original signal and can prove to be problematic. If the situation did contain purposeful or understood discontinuities, it may be important to preserve these trends and account for them instead of distorting them. For example, imagine a naval vessel that undergoes routine maintenance. If the connections of the panels were tightened at each inspection, the data would show that the panel would be self-healing because tightening the boundary conditions increases the stiffness of the structure. In this case, engineers knowingly introduced new behaviour into the system, but an automated SHM assessment system may see these trends in the data as increased noise or bias.

Statistical Filters

Statistical filters were also applied to discard any extraneous values. The idea behind using such a filter is to remove extreme values that may be affecting the prognostics but still preserve the datas original behaviour. The results from the statistical filters only served to narrow the variance of each prognostics plot. The locations of the peak values and entire range of predictions remained the same.

5.3   Variability

The prognostics results of both filters led us to conclude that the noise is not the primary reason for the flawed results. The results from the filters show that the feature values and feature rates themselves are not what they should be to make accurate and precise predictions. It is hypothesized that the chief source of variability comes from multiple sources of misrepresentations of the genuine panel behaviour. What appears to be happening overall is that the selected sensor pairs are trying to make sound predictions all while they are each individually faced with competing noise levels, α behaviours, environmental conditions, and poor testing procedures. This section will address each extraneous factor that contributes to the damage sensitve feature's variability.

5.3.1   Testing Environment

Some sources of variability came from the actual testing environment. An example of environmental induced variability would be variability from the panels temperature fluctuations. During testing, there was not enough time to test all the panels and give each panel sufficient time to reach a controlled temperature value before data collection. Therefore, the total strain signal recorded by the sensors is a combination of mechanical strains and inconsistent thermal strains.

We would like to only examine increasing strain values because of changes in the

material and geometric properties, but influences from thermal strains obscures this relationship. Unfortunately, the SHM system so far does not factor out the temperature induced strains. This shortcoming serves to be problematic when the vibration based features are derived from inaccurate strain values. Damage detection may incorrectly detect more or less damage depending on the level of uncontrolled temperature variations. Moreover, damage prognosis may produce faulty predictions from the affected vibration based features. Charles Farrar in his studies with the I-40 Bridges goes into great detail of the effects temperature differentials can have on vibration tests and modal parameters.[**?**]

5.3.2 Testing Procedures

Some sources of variability came from the actual testing procedures. An example of a testing procedure induced variability would be variability from any tampering of the test fixture. This is thought to have occurred with Panel 7. UCSD representatives were not present for the entirety of testing for Panel 7. After all the data were collected from Panel 7, several unusually large decreases in the Mahalnobis distances occurred in the time frame where testing was left to Applied Sciences employees and Hi-Test Laboratories technicians. Because the panel is not self-healing, it is hypothesized that the boundary conditions were tightened at several points during the test. Tightening the boundary conditions will increase the overall stiffness of the system. If the boundary condition rigidity is not consistently maintained, changes in the boundary condition will conflictingly influence the data.

As an alternative to controlling the end conditions, allowing the end conditions to freely decay is another way to control the system. Degradation of the end conditions could be associated to overall damage of the system. Decreases in stiffness will not only be represented in degradation of the panels properties, but also be represented in degradation of the panels boundary conditions. The latter means of working with the end conditions during testing was the approach we intended to model. Unfortunately, Applied Sciences employees and Hi-Test Laboratories may not have been aware of our choice to include boundary condition decay in the model for damage and may

have chosen the former method of controlling the experimental arrangement.

5.3.3   Model Correlation

Last but not least, the most obvious misalignment exists in the original assumptions. Both the indirect and the direct model were linearized through the assumption that α equals two. This assumption did not hold up when a nonlinear fit was performed on the data to solve for the empirical constants.

If the true value of α is less than 2 but we use the linearized model, our prediction with the linearized model will be greater than what would actually be observed giving us non-conservative predictions

If the true value of α is greater than 2 but we use the linearized model, our prediction with the linearized model will be less than what would actually be observed giving us conservative predictions.

Let us start with the equation:

$$t_f = t_c + \frac{R_c^{1-\alpha}}{\kappa * (\alpha - 1)} = t_c + \frac{R_c^{-(\alpha-1)}}{\kappa * (\alpha - 1)} = t_c + \frac{1}{\kappa * (\alpha - 1) * R_c^{\alpha-1}} \tag{5.1}$$

For $\alpha < 2$

$$t_f = t_c + \frac{1}{\kappa * ((\alpha < 2) - 1) * R_c^{(\alpha<2)-1}} = t_c + \frac{1}{\kappa * (\# < 1) * R_c^{\#<1}} \tag{5.2}$$

For $\alpha = 2$

$$t_f = t_c + \frac{1}{\kappa * ((\alpha = 2) - 1) * R_c^{(\alpha=2)-1}} = t_c + \frac{1}{\kappa * R_c} \tag{5.3}$$

For $\alpha > 2$

$$t_f = t_c + \frac{1}{\kappa * ((\alpha > 2) - 1) * R_c^{(\alpha>2)-1}} = t_c + \frac{1}{\kappa * (\# > 1) * R_c^{\#>1}} \tag{5.4}$$

Now, let us assign values to R_c, α, t_c, and κ and examine the time of failure predictions.

$R_c = .0128$

$t_c = 100$

$k = .0348$

$\alpha_1 = 1.5$

$\alpha_2 = 2.5$

For $\alpha = \alpha_1 = 1.5 < 2$

$$t_f = 100 + \frac{.0128^{1-\alpha_1}}{.0348 * (\alpha_1 - 1)} \tag{5.5}$$

$$t_f = 100 + \frac{.0128^{1-1.5}}{.0348 * (1.5 - 1)} = 608 \tag{5.6}$$

For $\alpha = \alpha_2 = 2.5 > 2$

$$t_f = 100 + \frac{.0128^{1-\alpha_2}}{.0348 * (\alpha_2 - 1)} \tag{5.7}$$

$$t_f = 100 + \frac{.0128^{1-2.5}}{.0348 * (2.5 - 1)} = 13329 \tag{5.8}$$

For $\alpha = 2$

$$t_f = 100 + \frac{.0128^{1-\alpha}}{.0348 * (\alpha - 1)} \tag{5.9}$$

$$t_f = 100 + \frac{.0128^{1-2}}{.0348 * (2 - 1)} = 2345 \tag{5.10}$$

If the true behavior positive feedback behavior is governed by an exponential α constant that is greater than two, the predictions will ideally begin underpredicting time of failure. Each future prediction will self-correct to greater values until the true time of failure is reached. This behaviour is the preferable case, for it represents a conservative damage prognosis. This behaviour is undesirable and embodies a non-conservative damage prognosis. If the true behavior

positive feedback behavior is governed by an exponential α constant that is less than two, the linearized predictions will ideally begin overpredicting time of failure. Each future predictions will self-correct to lesser values until the true time of failure is reached.

5.3.4 Empirical Constants

The linearized model reduces the number of unknowns in the problem. With the current tools developed for this SHM system, incorporating empirical constants in the blind prognosis algorithm would not be practical. The empirical constants cannot accurately be solved for if the point of failure is not known because the failure asymptote is defined by the empirical constants. Fits that occur in a panel's infancy will be poor and the empirical constants will be far from their true values. As the damage progresses, and more data is added, the estimates will improve. Only when the panel is close to failure will the estimated constants be close to their true value and the failure predictions will become strong. The direct method in this experiment partially uses this methodology but serves as a stepping stone for possible extension of this research.

5.4 Extensions

5.4.1 Damage Location

Through examining the particular sensor pairs used after data compression in Table 3.1 and Table 3.2, it is clear that there are sensors that appear more frequently than others. Mapping the sensor pairs on the panel and comparing their relative location to damage shows two useful trends. Sensor pairs that are in the vicinity of damage generally have the largest observed Mahalanobis distance values. Furthermore, sensor pairs that have disparately distant observed strain values relative to each other are also selected for prognosis. For example, the sensors pairs chosen for prognosis were either one of two cases. Either the sensor pairs were both close to observed composite damage, or one was close to the mid-span where the strains were large and the other was close to the fixed boundary condition where the strains were relatively smaller.

This trend could possibly be used to locate damage with the existing SHM system. Engineers can examine the observed Mahalnobis distance values and not only detect damage but also triangulate damage by mapping them back to the panel.
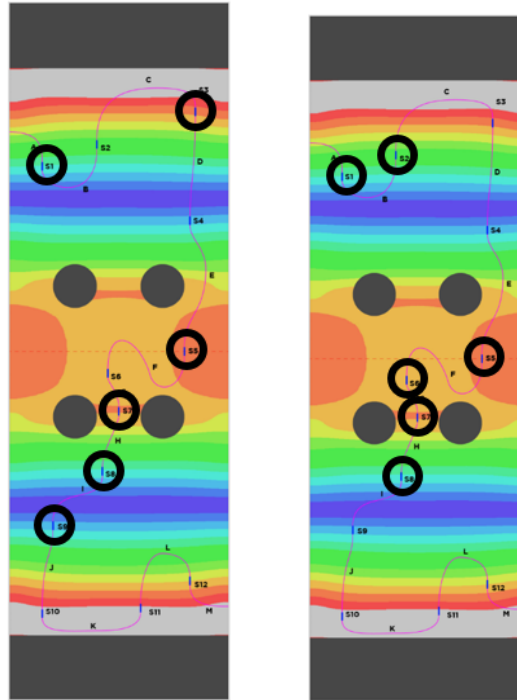

Figure 5.1. Selected sensor pair locations Panel 5 (Left) and Panel 7 (Right)

5.4.2   Monte-Carlo Simulation

It was previously mentioned that the empirical constants displayed a wide range of values amongst all the sensor pairs. Variation in the α values particularly introduced deviations away from the linearized model. Running the prognostics through a monte-carlo simulation of possible α and κ values could help engineers understand the impact the empirical constants have on prognostics. The results of a monte-carlo simulation could then help in determining the statistical properties of time of failure based on the input statistical properties. With an established empirical constant and prognostics relationship, uncertainty bounds can begin to be established at each prognostic result to aid in making up-to-date time of failure decisions. Additionally, these uncertainty bounds can better be quantified than the methods used in this

research.

The monte-carlo simulation procedure could be as follows. First, distributions of the empirical constants must be established. From the solved κ and α values, a PDF can be fitted to model their variance. Next, noisy sensor pair data sets can be created with a range of empirical constants. Prognostics can then run on the fictions data sets and hypothetical time of failure predictions can be made. The simulation would then continue this process with different empirical constant values that conform to the observed distribution of their values until the solution converges to the best combinations of empirical constants that best predict time of failure. One of the best solutions will indeed be the case that was assumed where all the α values are two. However, other solutions will also be brought to light. Perhaps a solution will be one where the mean α value is two. The results from all the monte-carlo simulations together can then be organized to depict hidden trends. Engineers will be able to understand how the predictions change with deviations away from the best solutions. Moreover, recognizable trends can help establish more precise confidence levels on predictions.

5.4.3 Local Regression Techniques

Better results may be obtained from different processes entirely. The indirect method used the backwards finite difference to calculate the feature rates but there are other approaches that can be used to calculate an observed rate at an observed time. Some ideas come from different local regression techniques. The prognostics developed previously implemented a linear fit between two observed feature values at two different observed damage levels. The solved rate would be the slope of the line connecting the two points. Better rate data may be produced if more points were included in this rate estimate process. Additional points can come from the same damage levels or even past damage levels.

Because the backwards finite difference is an underestimate of the observed rate at the current damage level, these particular points that are chosen to be part of the regression can be selected in a manner that accounts for the underestimate. Additional points can forcefully

increase the rate to a value greater than the rate of the backwards finite difference. Moreover, each point can be given different weights to influence the estimated best fit line. These ideas come from the locally estimated scatter plot smoothing (LOESS) and locally weighted estimated scatter plot smoothing (LOWESS) techniques. After the selected points have been smoothed by a fit line, the rate can be derived from the slope. Equally, instead of best fit lines(polynomials of order 1), nonlinear functions could be approximated from the selected points and a nonlinear least squares regression can be performed to calculate the rates.

5.4.4 Data Normalization

If nothing can be done to control competing noise levels, α behaviours, environmental conditions, and poor testing procedures, features and predictions should be normalized to account for them. Data normalization can help uncover the damage sensitive response from extraneous non-damaging influences. Equivalently, it can remove some sources of variability by factoring into consideration the non-damaging related influences over the feature, feature rates, and predictions. There are two general approaches to data normalization: [43]

- Cases when the source of variability can be measured

- Cases when the sources of variability cannot be measured

Some times the changes in the damage sensitive feature caused by damage are orthogonal to changes in the damage sensitive feature because of some source of variability. For this case, the source variability many not need to be measured.

The source variability needs to be measured when changes in the damage sensitive feature caused by damage are similar to changes in the damage sensitive feature because of some source of variability. All of the sources of variability in the previous sections are of this type. System level damage is defined so loosely in this thesis that many extraneous sources of variability can imitate damage within the feature. Furthermore, the feature is compressed into a scalar number
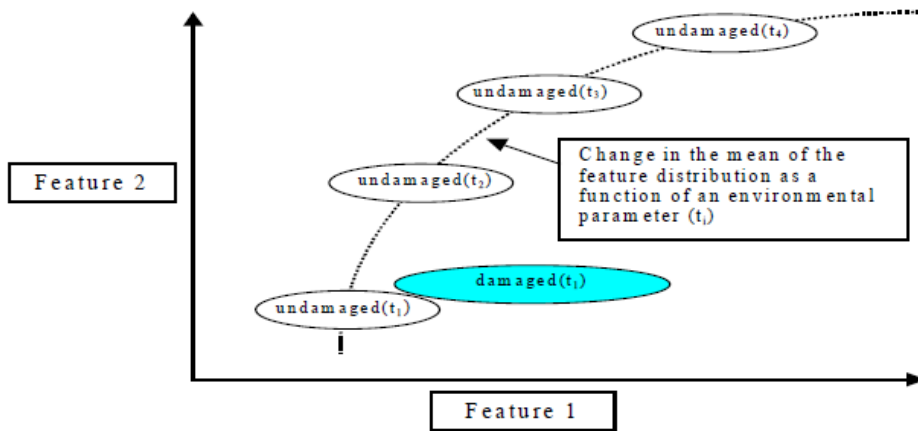
Figure 5.2. Changes in the feature caused by damage are orthogonal to changes in the feature because of some source of variability. [43]

by taking the Mahalanobis distance of peak shifts so much information about the entire system is lost.
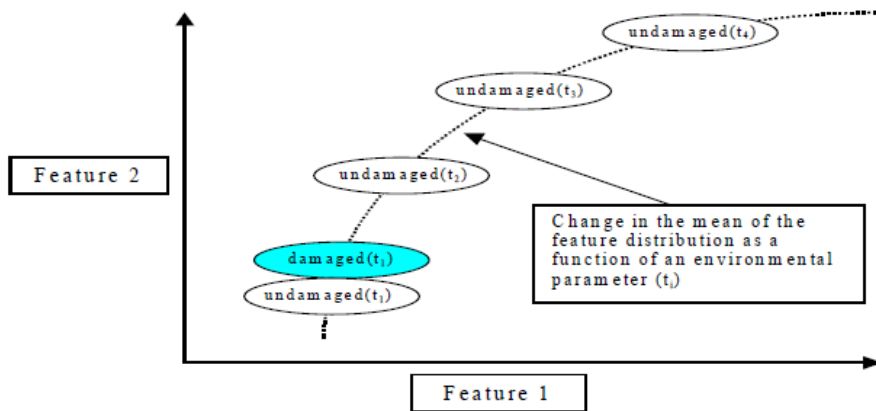

Figure 5.3. Changes in the feature caused by damage are similar to changes in the feature because of some source of variability. [43]

5.4.5   Machine Learning

So far, each of the noted sources of variability and addressed improvements belong to a distinct step in the SHM system. Variability in the testing environment represent holes in the operational evaluation that were not originally considered or taken into account. Variability in the testing procedure embody a misrepresented operational evaluation. Poor model correlation

86

can be tied to an insufficient DAQ system that failed to capture the positive feedback behavior. Filters are attempts made to improve the DAQ system. Equally, local regression techniques can be used to increase feature accuracy and decrease variability. With improved awareness of damage and extraneous factor sensitivity, data normalization on the feature will help to expand feature assessment and classification. Now, statistical model improvements must be defined.

It is clear that the statistical model did not perform its intended role. Prognostics was unable to consistently determine the remaining useful life of the structure, and time of failure predictions could not be classified into the right categories. For this thesis, there are three categories for time of failure predictions: 1.) Under predictions; 2.) Over prediction, and 3.) Accurate predictions. Each category was observed globally and locally. Globally, Panel 7's indirect method results were accurate, Panel 7's direct method results were over predictions, and Panel 5's direct method results were under predictions. Local damage level prognosis PDFs also had peaks that situated close to failure, far above failure, and far below failure.

The statistical model only involved selecting time of failure predictions from the data from ten damage indicative sensor pairs. The mean predictions were then fit into a normal PDF to produce a series of probabilistic prediction at each damage level. A more advanced post-processing or statistical feature chategorization procedure is needed to produce more conclusive results.

Different computer science techniques can be used to organize and sort through the data. Machine learning can give the SHM system the ability to make calculated decisions about the legitimacy of the data. One machine learning technique was used in the existing SHM system. It removed sensor pairs that were not indicative of damage. Similar techniques can be applied to disregard feature data, feature rates, or time of failure predictions that are poorly valued. During data processing time of failure predictions that were negative were disregarded. This idea can be extended further by even disregarding time of failure predictions that exist prior to the current observed damage level. Another machine learning algorithm can be used to sift through the feature or feature rate values. For example, some rates can be given less weight or some rates

can be omitted altogether given that they are less than the mean or median rate value from the previous damage level. Effectively, this machine learning technique will help to account for the noise in the rates by devaluing small valued rates that do not indicate damage evolution.

First, the uncertainty and variability around a prediction should be known. These statistical properties can be defined through the uncertainty and variability surrounded by the feature or feature rate the prediction is derived form. Next, the prediction can be placed into a statistical framework to assess the validity of a prediction. Based on the predictions statistical properties, ideally a prediction can be assessed as conservative, non-conservative, or accurate with some level of confidence. A hypothesis test that can reach a correct SHM assessment with the least probability of conservative and non-conservative predictions should be used. Conservative predictions are costly and threaten homeland security. Non-conservative predictions are dangerous for the crew onboard a naval vessel. More data may need to be gathered more frequently to minimize such predictions.

Prediction assessments can then be made based on the prediction deviating away from some normal operating condition. If the prediction space is well understood and the influences of competing noise levels, α behaviours, environmental conditions, and poor testing procedures on the predictions are known, the predictions can then be classified as conservative, non-conservative, or accurate.

It is known that predictions in the beginning will generally be poor representations of actual time of failure due to the noise levels overcoming the calculated observed rates. The statistical properties of the predictions will then show significant variability making the categorization process difficult. As more data is collected, categorization will become easier.

The underlying assumption to a positive feedback rate based prognosis method is that the rate of change of a damage sensitive feature is self-accelerating, and as failure is approached the evolution of a damage sensitive feature increases to infinity. When failure is eminent, the self-accelerating behavior will dominate over any noise present. It is safe to say that predictions will do the same and the predictions will be easier to classify because the noise will not contribute

88

to the prediction's variability. The positive feedback behavior will dominate over the noise and produce definitive statistical properties

5.5 Conclusion

There are two key objectives in Phase II of SBIR N111-053. One objective is to prove the viability of using FBG sensors in a fatigue loading environment. The other aim is to extend Yeager's SHM system beyond damage detection into damage prognosis.[42]

The FBG sensor arrays survived the fatigue environment and remained connected throughout the test on each of the specimens. No indication of fatigue damage or wear-out of the sensor array or connections were observed.

With the array surviving the fatigue environment, the data captured was processed using the existing Phase I SHM algorithm. Yeager's SHM algorithm successfully detected fatigue damage in the form of increased Mahlanobis distances feature values. Observed damage modes include, matrix cracking, delamination, bolt bearing damage, crack formation, crack propagation, and boundary condition weakening.

The end success was focused on developing a failure prognostics tool. Once developed, the tool was applied to a series of test specimens. The linear positive feedback failure forecast method made crude but moderately accurate time of failure predictions of a FRP panel subjected to cyclic fatigue loading. What appeared to happen overall is that sound predictions are trying to be made while the data is faced with competing noise levels, α behaviours, environmental conditions, and poor testing procedures. With different combinations of variability, prognostics will have unique observable trends. Overall, the experimental tests in thesis showed that Voight's original positive feedback mechanism can forecast fatigue failure, but considerable improvements on the SHM process will need to be made to produce accurate and precise results. It may be entirely possible that the damage prognosis method used in this thesis can produce accurate and precise results for the functioning onboard real-time assessment SHM strategy. The SHM system

for the function a naval submersible vessel is a real-time assessment strategy that gathers large amounts of data and conducts damage prognosis frequently. Accurate time of failure predictions with high confidences levels may be forecasted earlier than what was seen in the test results given that data demands are satisfied. To that end, it is worth investigating, testing, verifying, and validating the power law positive feedback linearized failure forecast method for a real-time damage prognosis SHM system.

Appendix A

Median Predictions

The statistical data driven prognosis approach used compresses a sensor pairs time of failure predictions into one mean time of failure prediction at each damaged level. Let us examine the results if the median time of failure prediction was chosen instead.

Figures A.1, A.2, A.3, A.4, A.5, A.6, A.7, and A.8 in the Appendix shows the prognostics plots when the median time of failure prediction is used instead of the mean prediction. The median predictions are consistently sooner than the mean time of failure predictions. Because the predictions are calculated from the feature values and the feature rates, it is safe to say that the feature values and feature rates also have median values that are consistently larger than the mean feature and and feature rate values.

It is unsure why the features do not have the similar or close in value mean and median values. Because the feature data sets have distributions where the mean and median values are not inline, so will the feature rates.

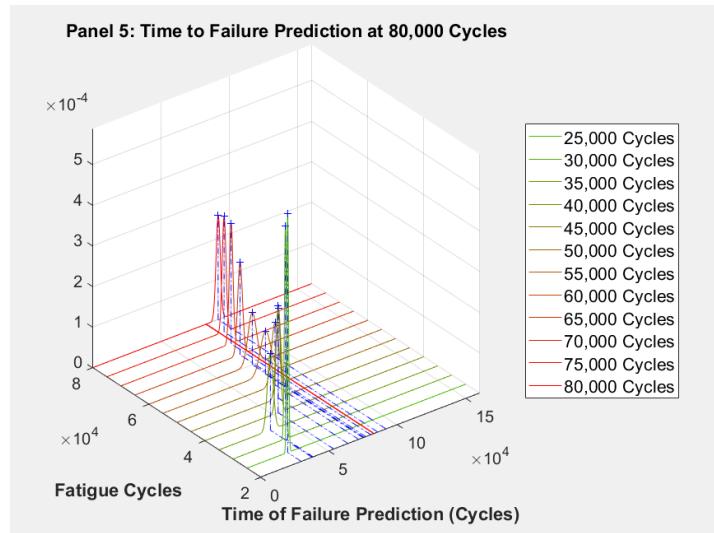**Panel 5 Indirect Method Plots (Median)**

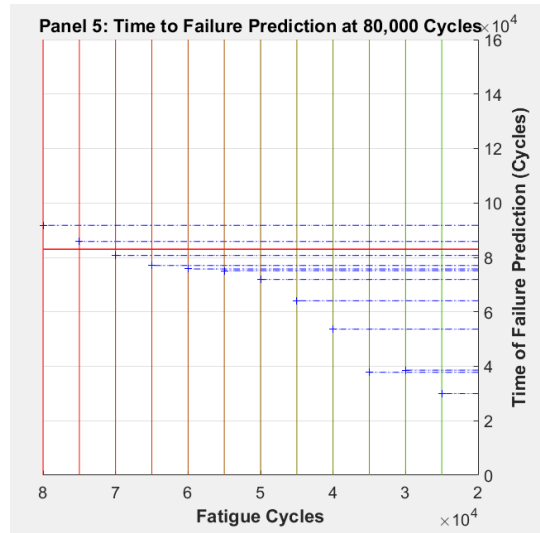**Figure A.1.** Prognosis evolution plot for Panel 5 (Indirect-Median).

Figure A.2. Prognosis evolution plot(Top View) for Panel 5 (Indirect-Median).
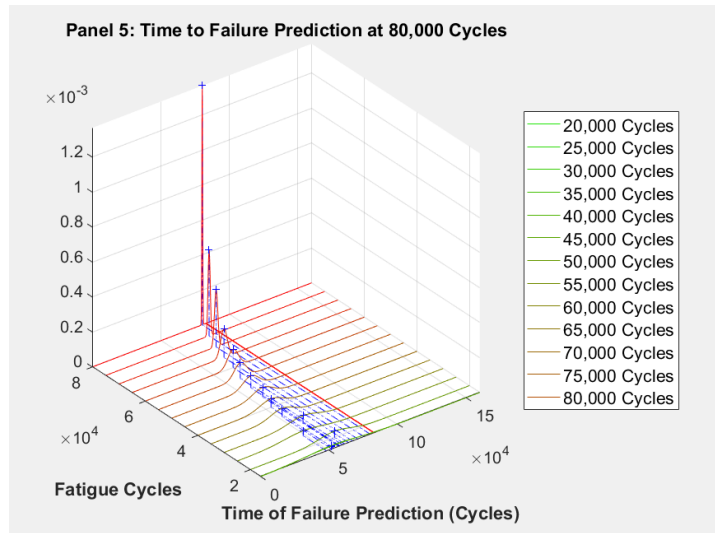
Panel 5 Direct Method Plots (Median)

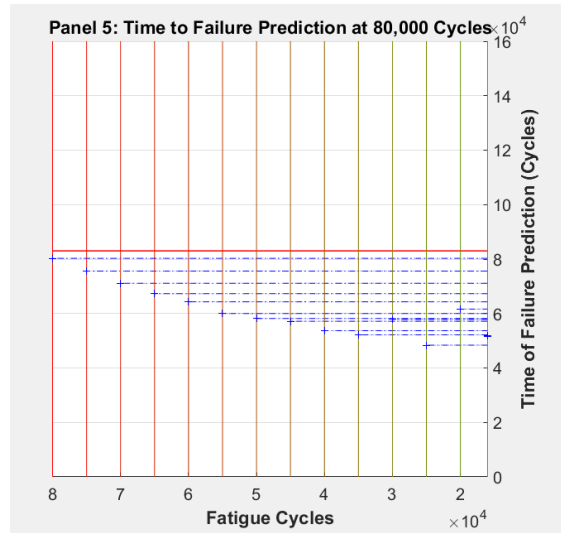**Figure A.3.** Prognosis evolution plot for Panel 5 (Direct-Median).

Figure A.4. Prognosis evolution plot(Top View) for Panel 5 (Direct-Median).
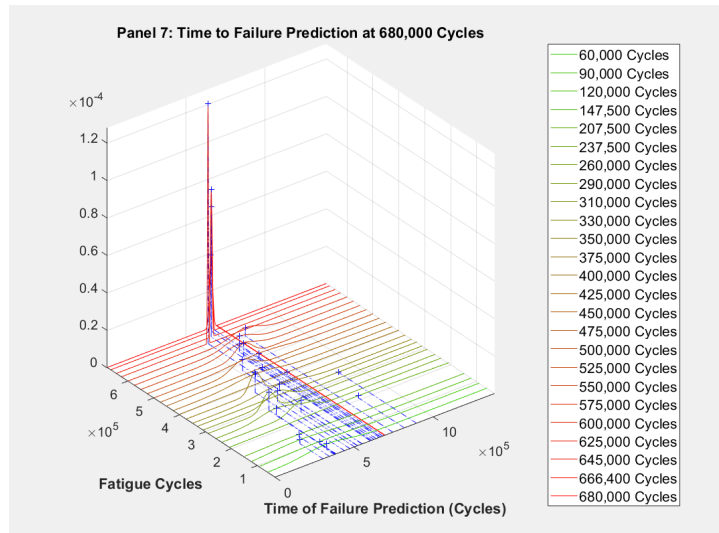
Panel 7 Indirect Method Plots (Median)

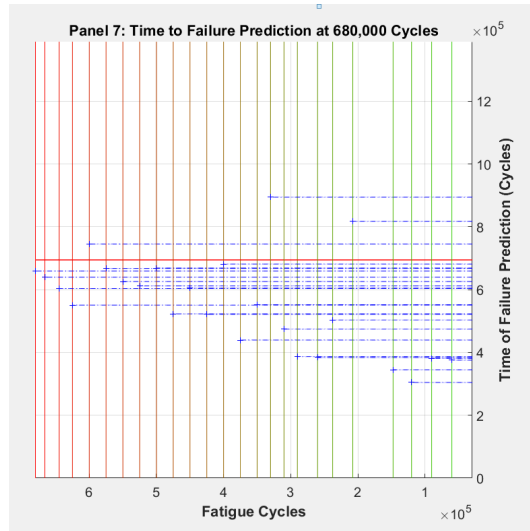**Figure A.5.** Prognosis evolution plot for Panel 7(Indirect-Median).

Figure A.6. Prognosis evolution plot(Top View) for Panel 7(Indirect-Median).
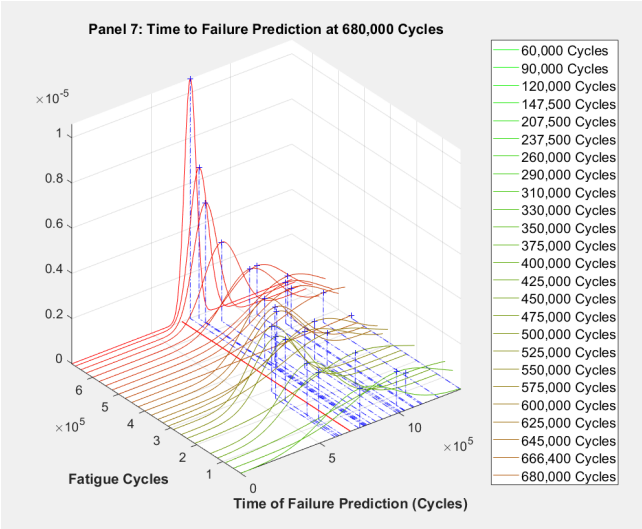
Panel 7 Direct Method Plots (Median)

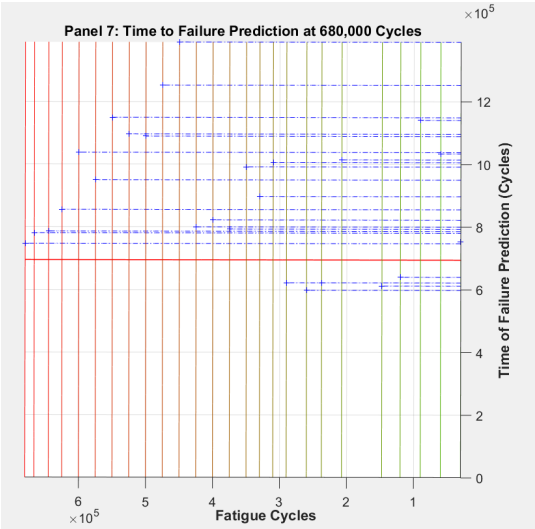**Figure A.7.** Prognosis evolution plot for Panel 7(Direct-Median).

Figure A.8. Prognosis evolution plot(Top View) for Panel 7(Direct-Median).

Bibliography

[1] Farrar CR; Worden K. *An introduction to structural health monitoring*. Philos Trans Roy Soc London A: Math Phys Eng Sci. 2007;365(1851):303315.

[2] Worden, Keith; Farrar, Charles; Manson, Graeme. *The Fundamental Axioms of Structural Health Monitoring*. Proceedings of The Royal Society A: Mathematical, Physical and Engineering Sciences. 463. 1639-1664. 10.1098/rspa.2007.1834.

[3] Farrar, Charles; Worden, Keith. *Structural Health Monitoring A Machine Learning Perspective.*. John Wiley Sons, LTD 10.1002/9781118443118.

[4] Sohn H; Farrar C; Hemez F; Shunk D; Stinemates D; Nadler B; Czarnecki J. *A review of structural health monitoring literature: 1996 2001*. 2003. Los Alamos, NM: Los Alamos National Laboratory.

[5] Farrar, Charles; Sohn, Hoon; Park, Gyuhae. *A statistical pattern recognition paradigm for structural health monitoring*. 9th ASCE Specialty Conference on Probabilistic Mechanics and Structural Reliability

[6] Dervilis, Nikolaos; Antoniadou, Ifigeneia; Barthorpe Robert J; Cross, Elizabeth; Worden, Keith. *Robust methods for outlier detection and regression for SHM applications*. International Journal of Sustainable Materials and Structural Systems. 2. 3. 10.1504/IJSMSS.2015.078354.

[7] Worden, Keith; W. Allen, David; Sohn, Hoon; W. Stinemates, Daniel; Farrar, Charles *Extreme Value Statistics for Damage Detection in Mechanical Structures*.

[8] Farrar, Charles; Lieven, Naj. *Damage prognosis: The future of structural health monitoring*. Philosophical transactions. Series A, Mathematical, physical, and engineering sciences. 365. 623-32. 10.1098/rsta.2006.1927.

[9] Farrar, Charles; Lieven, Naj. *Damage prognosis: The future of structural health monitoring*. Philosophical transactions. Series A, Mathematical, physical, and engineering sciences. 365. 623-32. 10.1098/rsta.2006.1927.

[10] Farrar, Charles; Sohn, Hoon; Hemez, Francois; Anderson, Mark; Bement, Matthew; Cornwell, Phillip; W. Doebling, S; Lieven, Naj; Robertson, Amy; Schultze, John *Damage Prognosis: Current Status and Future Needs*. Philosophical transactions. Series A, Mathematical, physical, and engineering sciences. 365. 623-32. 10.1098/rsta.2006.1927.

[11] Inman, Daniel; Farrar, Charles; Lopes Junior, Vicente; Steffen, Jr, Valder. *Damage Prognosis: For Aerospace, Civil and Mechanical Systems*. 10.1002/0470869097.

[12] Voight, Barry *A method for prediction of volcanic eruptions*. Nature 332, 125-130. Nature. 332. (1988) 125-130. 10.1038/332125a0.

[13] DeAngelis DL, Post WM, Travis CC *Positive feedback in natural systems*. Berlin, Germany: Springer

[14] Arthur WB. *Positive feedbacks in the economy*. Sci. Am. 262, 9299

[15] De Long JB, Shleifer A, Summers LH, Waldmann RJ. *Positive feedback investment strategies and destabilizing rational speculation*. J. Finance 45, 379395. doi:10.1111/j.1540-6261.1990.tb03695.x

[16] Biggs M *Positive feedback in collective mobilization: the American strike wave of 1886*. Theory Soc. 32, 217254. doi:10.1023/A:1023905019461

[17] Corcoran, Joseph. *Rate-based structural health monitoring using permanently installed sensors.*. Proceedings. Mathematical, physical, and engineering sciences vol. 473,2205 (2017): 20170270. doi:10.1098/rspa.2017.0270

[18] Leung, Michael Corcoran, Joseph Cawley, Peter and D. Todd, Michael. *Evaluating the use of Rate-based Monitoring for Improved Fatigue Remnant Life Predictions*. International Journal of Fatigue. 120. 10.1016/j.ijfatigue.2018.11.012.

[19] Ansari F *Fiber grating sensors*. Springer Netherlands. 10.1007/1-4020-3661-2

[20] Alan D. Kersey; Michael A. Davis; Heather J. Patrick; Michel Leblanc; K. P. Koo; C. G. Askins; M. A. Putnam; E. Joseph Friebele *Fiber grating sensors*. J. Lightwave Technol. 1997;15(8):14421463.

[21] Ghezzo, F.; Huang, Y.; Nemat-Nasser, S. *Onset of Resin Micro-Cracks in Unidirectional Glass Fiber Laminates with Integrated SHM Sensors: Experimental Results*. Structural Health Monitoring, 8(6), 477491. https://doi.org/10.1177/1475921709340976

[22] Shivakumar, K.; Emmanwori, L. *Mechanics of failure of Composite Laminates with an embedded Fiber optic Sensor*. Journal of Composite Materials, 38(8), 669-680.

[23] Shivakumar, K.; Emmanwori, L. *Failure mechanisms of a composite laminate embedded with a fiber optic sensor*. Journal of Composite Materials, 39(9), 777-798.

[24] Skontorp, Arne. *Effect Of Embedded Optical Fibers On The Structural Integrity Of Composites* . Journal of Composite Materials, 39(9), 777-798.

[25] M Measures, R; Glossop, Neil; Lymer, J; Leblanc, Michel; West, James; Dubois, S; Tsaw, W; Tennyson, Rod. *Structurally Integrated Fiber Optic Damage Assessment System For Composite Materials*. Applied optics. 28. 2626-33. 10.1364/AO.28.002626.

[26] de Oliveira R; Ramos CA; Marques AT. *Health monitoring of composite structures by embedded FBG and interferometric Fabry-Prot sensors*. Comput. Struct.. 2008;86(3): 340346.

[27] Majumder, Mousumi; Gangopadhyay, Tarun; Kumar Chakraborty Ashim; Dasgupta, Kamal; Bhattacharya, D.K. *Review Fibre Bragg Gratings in Structural Health MonitoringPresent Status and Applications*. Sensors and Actuators A: Physical. 147. 150-164. 10.1016/j.sna.2008.04.008.

[28] Peters, K *Full-spectrum FBG analysis of inhomogeneous, fast-varying strain effects*. In: Third Asia Pacific optical sensors conference. Sydney: International Society for Optics and Photonics; 2012. DOI:10.1117/12.916010

[29] Jang, Byeong-Wook; Park, Sang-Oh; Lee, Yeon-Gwan; Kim, Chun-Gon; Park, Chan Yik. *Detection of Impact Damage in Composite Structures Using High Speed FBG Interrogator*. Advanced Composite Materials - ADV COMPOS MATER. 21. 29-44. 10.1163/156855111X620874.

[30] Sunho Park, Taesung Park; Kyungseop Han *Real-Time Monitoring of Composite Wind Turbine Blades Using Fiber Bragg Grating Sensors*. Advanced Composite Materials, 20:1, 39-51, DOI: 10.1163/092430410X504198

[31] Murayama H; Kageyama K; Kamita K; *Structural health monitoring of a full-scale composite structure with fiber-optic sensors*. Adv Compos Mater. 2002;11(3):287297.

[32] Yeager, Mike; Todd, Michael; Gregory, William; Key, Chris. *IWSHM 2015: Assessment of embedded fiber Bragg gratings for structural health monitoring of composites*. Structural Health Monitoring. 16. 10.1177/1475921716665563.

[33] Doebling, S.W.; Farrar, C.R.; Prime, M.B.; Shevitz, D.W. *Damage identification and health monitoring of structural and mechanical systems from changes in their vibration characteristics: A literature review*. The Shock and Vibration Digest. 38. 295. 10.1177/0583102406065898.

[34] W. Doebling, Scott; Farrar, Charles; Prime, Michael; *A Summary Review of Vibration-Based Damage Identification Methods*. The Shock and Vibration Digest. 30. 91-105. 10.1177/058310249803000201.

[35] Farrar, C.R.; Baker, W.E.; Bell, T.M.; Cone, K.M.; Darling, T.W.; Duffey, T.A.; Eklund, A.; Migliori, A. *Dynamic characterization and damage detection in the I-40 bridge over the Rio Grande*. No. LA12767-MS. Los Alamos National Lab., Los Alamos, NM, USA, 1994.

[36] Farrar, Charles; Doebling, S.W.; Nix, D.A. *Vibration based structural damage identification*. Philosophical Transactions: Mathematical, Physical and Engineering Sciences Vol. 359, No. 1778, Experimental Modal Analysis (Jan. 15, 2001), pp. 131-149

[37] Montalvo, Diogo; M. M. Maia, N; Ribeiro, A. *A Review of Vibration-based Structural Health Monitoring with Special Emphasis on Composite Materials*. The Shock and Vibration Digest. 38. 295. 10.1177/0583102406065898.

[38] Kessler SS; Spearing SM; Attala MJ *Damage detection in composite materials using frequency response methods*. Compos Part B: Eng. 2002;33(1):8795.

[39] Masjedian, M.H.; Keshmiri, Mehdi. *A review on operational modal analysis researches: Classification of methods and applications*. IOMAC 2009 - 3rd International Operational Modal Analysis Conference. 707-716.

[40] Bendat, Julius S; Allan G. Piersol. *Random Data: Analysis and Measurement Procedures*. New York: Wiley, 2000. Print.

[41] Lutes, L D; Shahram Sarkani. *Random Vibrations: Analysis of Structural and Mechanical Systems*. Amsterdam: Elsevier Butterworth-Heinemann, 2004. Print.

[42] Mike Yeager; Anthony Whitaker; Daniel A. Whisler; Hyonny Kim; William Gregory; Chris Key; Michael Todd *Binary hypothesis-based impact damage detection for composite material system embedded with fiber Bragg gratings*. Advanced Composite Materials, 26:sup1, 79-92, DOI: 10.1080/09243046.2017.1314063 2017.

[43] Farrar, Charles; Sohn, Hoon; Worden, K. *Data normalization: a key to structural health monitoring*. Advanced Composite Materials, 26:sup1, 79-92, DOI: 10.1080/09243046.2017.1314063 2017.